

**UNIVERSITY OF GAZİANTEP  
GRADUATE SCHOOL OF  
NATURAL & APPLIED SCIENCES**

**THE INVESTIGATION OF THERMOLUMINESCENCE  
INTENSITY-DOSE RESPONSE RELATION OF THE TOOTH  
ENAMEL AFTER DIFFERENT ANNEALING TEMPERATURES**

**M.Sc. THESIS**

**IN**

**PHYSICS ENGINEERING**

**BY**

**SİNEM MERVE YILMAZ**

**JULY 2017**

**JULY 2017**

**M.Sc. in Physics Engineering**

**SİNEM MERVE YILMAZ**

**The Investigation of Thermoluminescence Intensity-Dose Response Relation of  
the Tooth Enamel After Different Annealing Temperatures**

**M.Sc. Thesis**

**in**

**Physics Engineering**

**University of Gaziantep**

**Supervisor**

**Assoc. Prof. Dr. Hüseyin TOKTAMIŞ**

**by**

**Sinem Merve YILMAZ**

**July 2017**



© 2017 [Sinem Merve YILMAZ]

REPUBLIC OF TURKEY  
UNIVERSITY OF GAZIANTEP  
GRADUATE SCHOOL OF  
NATURAL & APPLIED SCIENCES  
PHYSICS ENGINEERING

**Name of the Thesis:** The Investigation of Thermoluminescence Intensity-Dose Response Relation of the Tooth Enamel at Different Annealing Temperatures


**Name of the student:** Sinem Merve YILMAZ

**Exam date:** 31.07.2017

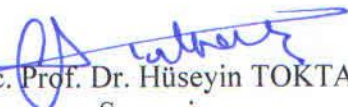
Approval of the Graduate School of Natural and Applied Sciences

  
Prof. Dr. A. Necmeddin YAZICI  
Director

I certify that this thesis satisfies all the requirements as a thesis for the degree of Master of Science.

  
Prof. Dr. Ramazan KOÇ  
Head of Department

This is to certify that we have read this thesis and that in our consensus opinion it is fully adequate, in scope and quality, as a thesis for the degree of Master of Science.

  
Assoc. Prof. Dr. Hüseyin TOKTAMIŞ  
Supervisor

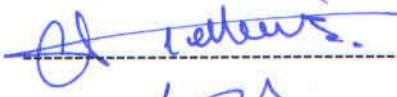
Examining Committee Member

Signature

Assoc. Prof. Dr. Vural Emir KAFADAR

  
-----

Assoc. Prof. Dr. Hüseyin TOKTAMIŞ

  
-----

Assist. Prof. Dr. Necmettin NUR

  
-----

**I hereby declare that all information in this document has been obtained and presented in accordance with academic rules and ethical conduct. I also declare that, as required by these rules and conduct, I have fully cited and referenced all material and results that are not original to this work.**

**Sinem Merve YILMAZ**

## **ABSTRACT**

### **THE INVESTIGATION OF THERMOLUMINESCENCE INTENSITY-DOSE RESPONSE RELATION OF THE TOOTH ENAMEL AFTER DIFFERENT ANNEALING TEMPERATURES**

**YILMAZ, Sinem Merve**

**M.Sc. in Physics Engineering**

**Supervisor: Assoc. Prof. Dr. Hüseyin TOKTAMIŞ**

**July 2017**

**64 pages**

Thermoluminescence (TL) is the natural light phenomenon emitted from an insulator or wide band gap semiconductor after absorbing some energy from an external radiation source when it is stimulated by thermal excitation. Tooth enamel is the hardest part of tooth and protects the dentine. In terms of its weight, it consists of 95% inorganic minerals, 1% organic minerals, and 3% water. Fluorapatite  $\text{Ca}_5\text{F}(\text{PO}_4)_3$  is an important mineral in tooth enamel. Due to the fact that the effective atomic number of fluorapatite is nearly the same with human calcified tissues, it is a candidate of important thermoluminescence dosimeter (TLD) material. In this thesis, thermoluminescence (TL) intensity-dose response relation of fluorapatite mineral in tooth enamel under the different annealing temperatures were investigated and then analyzed its thermoluminescence glow curve peaks with a computer programs. This study reveals that the fluorapatite mineral extracted from tooth enamel shows TL properties. Annealing of the sample at different temperatures affects the TL output-dose response relation. A good linearity in dose response is observed in the samples annealed at 400 °C and 700 °C. And also, dose variation differently changes the trap positions at different annealing temperature.

**Key Words:** Thermoluminescence, tooth enamel, dosimeter, fluorapatite

## ÖZET

# DİŞ MİNESİNİN FARKLI TAVLAMA SICAKLIKLARINDA TERMOLÜMİNESANS ŞİDDET-DOZ İLİŞKİSİ ÖZELLİKLERİNİN İNCELENMESİ

**YILMAZ, Sinem Merve**

**Yüksek Lisans Tezi, Fizik Müh. Bölümü**

**Tez Yöneticisi: Doç. Dr. Hüseyin TOKTAMIŞ**

**Temmuz 2017**

**64 sayfa**

Termolüminasans, bir radyasyon kaynağından enerji soğurmuş bir yalıtkan veya geniş bant aralığına sahip yarıiletken ısıtıldığında görülen doğal ışık olayıdır. Diş minesinin en sert kısmı olup dişin dentin kısmını korur. Ağırlığı bakımından diş minesinin %95 inorganik minerallerden, %3'ü suda ve %1'i ise organik minerallerden oluşur. Florapatit  $\text{Ca}_5\text{F}(\text{PO}_4)_3$  diş minesinde önemli bir apatit mineraldir. Florapatitin etkin atom numarası insanın kalsiyum yapılı organları ile neredeyse aynı olmasından dolayı önemli termolüminasans dozimetrik (TLD) materyaller için bir adaydır. Bu çalışmada, farklı tavlama sıcaklarında diş minesindeki florapatit mineralin termolüminasans şiddet doz ilişkisi araştırılmış ve ışıltama eğrisine etkileri bir bilgisayar programı yardımı ile analiz edilmiştir. Bu çalışma ile diş minesinden elde edilen florapatit mineralin termolüminasans özellikleri gösterdiği gözlemlenmiş ve numunenin farklı sıcaklarda tavlama termolüminasans (TL) şiddet- doz tepkisi ilişkisini etkilediği görülmüştür. Doz tepkisi deneyinde en iyi lineerlik 400 °C ve 700 °C de tavlama numunelerinde elde edilmiştir. Bunun dışında farklı tavlama sıcaklığında doz değişimi tuzak pozisyonlarını farklı bir şekilde etkilediği görülmüştür.

**Key Words:** Termolüminasans, diş minesinin, dozimetre, florapatit



*To me, my family, especially my mother ...*



## ACKNOWLEDGEMENT

The first person that I would like to thank to Assist. Prof. Dr. Hüseyin TOKTAMIŞ for helping and supporting me throughout the project. It is thanks to his meticulous care and painstaking exactness that the project has taken its present form. Furthermore, he has checked the whole project with remarkable patience, pointing out errors which might have otherwise gone unnoticed.

I am almost grateful to Mrs. Dilek TOKTAMIŞ for her patience, suggestion, advice and help in the preparation of this study.

I must say a special thanks to my deceased grandmother Afife Sevim YALBUZDAĞ, my mother Özlem YALBUZDAĞ and my sister Gözde Miray YILMAZ for supporting and encouraging me.

Another my special thanks to my dear friend Ali AKSOY for his patience.

## TABLE OF CONTENTS

<b>CONTENTS</b>	<b>Page</b>
<b>TABLE OF CONTENTS</b> .....	ix
<b>LIST OF FIGURES</b> .....	xii
<b>LIST OF TABLES</b> .....	xvi
<b>CHAPTER 1: INTRODUCTION</b> .....	1
<b>CHAPTER 2: LITERATURE SURVEY</b> .....	4
2.1. Tooth Structure .....	4
2.2. The Tooth Enamel .....	5
2.2.1. Tooth Enamel Histology.....	5
2.2.2. Tooth Enamel Morphogenesis.....	6
2.2.3. The Mineral Phase .....	7
2.3. Thermally Stimulated Luminescence (TL) .....	7
2.4. Dose Response .....	9
2.5. Annealing .....	14
<b>CHAPTER 3: EXPERIMENTAL PROCEDURE</b> .....	17
3.1. Material .....	17
3.2. Equipments .....	19
3.2.1. Radiation Source and Irradiator.....	19

3.2.2. TLD Reader .....	20
3.2.3. Annealing Furnace.....	21
3.2.4. Digital Balance .....	21
3.2.5. Digital Balance .....	22
3.3. Experimental Procedure .....	22
<b>CHAPTER 4: EXPERIMENTAL RESULTS AND DISCUSSIONS .....</b>	<b>23</b>
4.1. Glow Curve Variations .....	23
4.1.1. The Glow Curve Variation of Sample Annealed at 400 °C .....	24
4.1.2. The Glow Curve Variation of Sample Annealed at 500 °C .....	25
4.1.3. The Glow Curve Variation of Sample Annealed at 600 °C .....	26
4.1.4. The Glow Curve Variation of Sample Annealed at 700 °C .....	27
4.1.5. The Glow Curve Variation of Sample Annealed at 800 °C .....	28
4.1.6. The Glow Curve Variation of Sample Annealed at 900 °C .....	29
4.1.7. The Glow Curve Variation of Sample Annealed at 1000 °C .....	30
4.1.8. The Glow Curve Variation of Sample Annealed at 1100 °C .....	31
4.2. Variation of TL Peak Intensity .....	32
4.2.1. Variation of TL Peak Intensity of Sample at 400 °C .....	32
4.2.2. Variation of TL Peak Intensity of Sample at 500 °C .....	33
4.2.3. Variation of TL Peak Intensity of Sample at 600 °C .....	34
4.2.4. Variation of TL Peak Intensity of Sample at 700 °C .....	35
4.2.5. Variation of TL Peak Intensity of Sample at 800 °C .....	36
4.2.6. Variation of TL Peak Intensity of Sample at 900 °C .....	37

4.2.7. Variation of TL Peak Intensity of Sample at 1000 °C .....	38
4.2.8. Variation of TL Peak Intensity of Sample at 1100 °C .....	39
4.3. The Area Under The Curve .....	40
4.3.1. The Area Under The Curve Variations of Sample at 400 °C .....	40
4.3.2. The Area Under The Curve Variations of Sample at 500 °C .....	41
4.3.3. The Area Under The Curve Variations of Sample at 600 °C .....	42
4.3.4. The Area Under The Curve Variations of Sample at 700 °C .....	43
4.3.5. The Area Under The Curve Variations of Sample at 800 °C .....	44
4.3.6. The Area Under The Curve Variations of Sample at 900 °C .....	45
4.3.7. The Area Under The Curve Variations of Sample at 1000 °C .....	46
4.3.8. The Area Under The Curve Variations of Sample at 1100 °C .....	47
4.4. Peak Temperature .....	48
4.2.1. Variation of TL Peak Temperature of Sample at 400 °C .....	48
4.2.2. Variation of TL Peak Temperature of Sample at 500 °C .....	49
4.2.3. Variation of TL Peak Temperature of Sample at 600 °C .....	50
4.2.4. Variation of TL Peak Temperature of Sample at 700 °C .....	51
4.2.5. Variation of TL Peak Temperature of Sample at 800 °C .....	52
4.2.6. Variation of TL Peak Temperature of Sample at 900 °C .....	53
4.2.7. Variation of TL Peak Temperature of Sample at 1000 °C .....	54
4.2.8. Variation of TL Peak Temperature of Sample at 1100 °C .....	55
<b>CHAPTER 5: DISCUSSION AND CONCLUSION .....</b>	<b>56</b>
<b>REFERENCES .....</b>	<b>58</b>

## LIST OF FIGURES

<b>LIST OF FIGURES</b>		<b>PAGE</b>
<b>Figure 2.1</b>	Tooths of structure, parth of teeth.....	4
<b>Figure 2.2</b>	Structure of enamel.....	5
<b>Figure 2.3</b>	Typical thermoluminescence glow curve from a sedimentary K-feldspar sample given a beta dose of 8 Gy in addition to the natural dose.....	8
<b>Figure 2.4</b>	Examples of growth curves for three thermoluminescence samples. Curve A: The thermoluminescence dose response for the 100 °C peak in SiO <sub>2</sub> . Curve B: The dose response is linear, supralinear and sublinear for peak 5 from TLD-100 (LiF:Mg,Ti). Curve C: The dose response of TLD-400 (CaF <sub>2</sub> :Mn) in which supralinearity is very weak.....	10
<b>Figure 2.5</b>	Figure 2.8 Schematic dose response curves for several cases. Note that this is a log-log plot in which $f(D) = 1$ is indicated by a slope of 1 (viz. the dashed line).....	11
<b>Figure 3.1</b>	Sample of the tooth enamel .....	17
<b>Figure 3.2</b>	The powder tooth enamel sample .....	18
<b>Figure 3.3</b>	X-ray diffraction (XRD) pattern of tooth enamel .....	18
<b>Figure 3.4</b>	Radiation source installed in a 9010 optical dating system which is interfaced to a PC using a serial RS-232 port.....	19
<b>Figure 3.5</b>	TLD Reader.....	20
<b>Figure 3.6</b>	Basic block diagram of TLD reader .....	20
<b>Figure 3.7</b>	Annealing Oven .....	21

<b>Figure 3.8</b>	Digital Balance.....	21
<b>Figure 3.9</b>	Agate Mortar .....	22
<b>Figure 4.1</b>	Variation of shape of glow curves of the sample annealed at 400°C as a function of applied dose .....	24
<b>Figure 4.2</b>	Variation of shape of glow curves of the sample annealed at 500 °C as a function of applied dose .....	25
<b>Figure 4.3</b>	Variation of shape of glow curves of the sample annealed at 600 °C as a function of applied dose .....	26
<b>Figure 4.4</b>	Variation of shape of glow curves of the sample annealed at 700 °C as a function of applied dose .....	27
<b>Figure 4.5</b>	Variation of shape of glow curves of the sample annealed at 800 °C as a function of applied dose .....	28
<b>Figure 4.6</b>	Variation of shape of glow curves of the sample annealed at 900 °C as a function of applied dose .....	29
<b>Figure 4.7</b>	Variation of shape of glow curves of the sample annealed at 1000 °C as a function of applied dose.....	30
<b>Figure 4.8</b>	Variation of shape of glow curves of the sample annealed at 1100 °C as a function of applied dose .....	31
<b>Figure 4.9</b>	The TL peak intensity variation of the sample annealed at 400 °C as a function of applied dose .....	32
<b>Figure 4.10</b>	The TL peak intensity variation of the sample annealed at 500 °C as a function of applied dose .....	33

<b>Figure 4.11</b>	The TL peak intensity variation of the sample annealed at 600 °C as a function of applied dose .....	34
<b>Figure 4.12</b>	The TL peak intensity variation of the sample annealed at 700 °C as a function of applied dose .....	35
<b>Figure 4.13</b>	The TL peak intensity variation of the sample annealed at 800 °C as a function of applied dose .....	36
<b>Figure 4.14</b>	The TL peak intensity variation of the sample annealed at 900 °C as a function of applied dose .....	37
<b>Figure 4.15</b>	The TL peak intensity variation of the sample annealed at 1000 °C as a function of applied dose .....	38
<b>Figure 4.16</b>	The TL peak intensity variation of the sample annealed at 1100 °C as a function of applied dose .....	39
<b>Figure 4.17</b>	The area under the curve variations of the sample annealed at 400 °C as a function of applied dose .....	40
<b>Figure 4.18</b>	The area under the curve variations of the sample annealed at 500 °C as a function of applied dose .....	41
<b>Figure 4.19</b>	The area under the curve variations of the sample annealed at 600 °C as a function of applied dose .....	42
<b>Figure 4.20</b>	The area under the curve variations of the sample annealed at 700 °C as a function of applied dose .....	43
<b>Figure 4.21</b>	The area under the curve variations of the sample annealed at 800 °C as a function of applied dose .....	44

<b>Figure 4.22</b>	The area under the curve variations of the sample annealed at 900 °C as a function of applied dose .....	45
<b>Figure 4.23</b>	The area under the curve variations of the sample annealed at 1000 °C as a function of applied dose .....	46
<b>Figure 4.24</b>	The area under the curve variations of the sample annealed at 1100 °C as a function of applied dose .....	47
<b>Figure 4.25</b>	The peak temperature variations of the sample annealed at 400 °C as a function of applied dose .....	48
<b>Figure 4.26</b>	The peak temperature variations of the sample annealed at 500 °C as a function of applied dose .....	49
<b>Figure 4.27</b>	The peak temperature variations of the sample annealed at 600 °C as a function of applied dose .....	50
<b>Figure 4.28</b>	The peak temperature variations of the sample annealed at 700 °C as a function of applied dose .....	51
<b>Figure 4.29</b>	The peak temperature variations of the sample annealed at 800 °C as a function of applied dose .....	52
<b>Figure 4.30</b>	The peak temperature variations of the sample annealed at 900 °C as a function of applied dose .....	53
<b>Figure 4.31</b>	The peak temperature variations of the sample annealed at 1000 °C as a function of applied dose .....	54
<b>Figure 4.32</b>	The peak temperature variations of the sample annealed at 1100 °C as a function of applied dose .....	55



## LIST OF TABLES

<b>TABLES</b>		<b>Page</b>
<b>Table 3.1</b>	The Peak ID Extended Report of tooth enamel	18



## CHAPTER 1

### INTRODUCTION

The hardest part of tooth is tooth enamel and protects the dentine. In terms of its weight, it consists of 95% inorganic minerals, 1% organic minerals, and 3% water [1-3]. It is a complex biomaterial, a composite of elongated mineral crystallites in the form of biological apatite bonded by polymeric proteins and peptide chains saturated with water [4]. It has a hierarchical structure with crystals of hexagonal cross-section tightly packed into rods (prisms) (width~5 $\mu\text{m}$ ) [5] and enclosed by polymeric sheaths (width 0.1 $\mu\text{m}$ ) [4]. In 1964 about twenty inorganic elements except oxygen, hydrogen and carbon were found in tooth enamel. Hydroxyapatite,  $\text{Ca}_{10}(\text{PO}_4)_6(\text{OH})_2$ , and fluorapatite,  $\text{Ca}_5\text{F}(\text{PO}_4)_3$ , minerals are two major inorganic apatite minerals in tooth enamel. Apatites are found in the same family of compounds identified by an identical structure, albeit with dissimilar configurations. When fluor (F) ions substitute with OH in hydroxyapatite  $\text{Ca}_{10}(\text{PO}_4)_6(\text{OH})_2$ , fluorapatite minerals  $\text{Ca}_5\text{F}(\text{PO}_4)_3$  are formed [1-3,6]. Studies of related synthetic or natural compounds of tooth enamel apatite have given most of the present information about the tooth enamel apatite. Biological apatites contain some ions such as  $\text{CO}_3^{2-}$ ,  $\text{PO}_4^{3-}$ ,  $\text{OH}^-$  and  $\text{Ca}^{2+}$  and different forms of apatite may form with substituting of present ions [7]. P,  $\text{CO}_3$ , Mg, Cl, and K are the major and Fe, Zn, Sr, F, Ca and Na are the minor constituents in tooth enamel [8]. For all that, Zn, Sr, Si, F, S, Al and Fe are the trace elements in tooth enamel. Minor ingredients and trace elements have been created in tooth enamel throughout mineralization. The stability of apatite minerals has been generally achieved by the trace elements and minor ingredients [9].

A few researchers [10, 11-17] have investigated the thermoluminescence properties of synthetic and biological apatites. In the study of Secu et. al.[10], they pointed out the tooth enamel present a wide glow curve from 100 to 450 $^\circ\text{C}$  and TL signal in the 250-450 $^\circ\text{C}$  temperature region escalations with applied dose. They supposed that the thermoluminescence peaks below 300 $^\circ\text{C}$  are due to the impurities such as  $\text{Mn}^{+2}$  and trivalent rare earths impurities. For the thermoluminescence peaks between 300 $^\circ\text{C}$  and

400°C, the existence of some paramagnetic classes such as  $\text{CO}_2^-$ ,  $\text{CO}_3^-$  and  $\text{CO}^-$  revealed by EPR spectra of biological and synthetic apatite may cause higher TL peaks. Also they concluded the multifaceted assembly of the TL glow curve in tooth enamel had been recognized to the recombination of radiation induced  $\text{CO}_2^-$  radicals created from surface  $\text{CO}_2$  and or bulk  $\text{CO}_3$  impurities. The radiation-convincing signal in tooth enamel may include some  $\text{CO}_2^-$  species found in different locations [16]. Fukuda [18] investigated the some thermoluminescence properties of synthetic fluorapatite because the effective atomic number of synthetic fluorapatite is about 14 [19] and is nearly the same with that of human calcified tissues. A thermoluminescence glow curve with two leading peaks located at 100°C and 235°C was obtained.

Tooth enamel is one of the most known detector as vivo dosimetry [20]. The accumulated dose in tooth enamel was investigated by some researchers [10, 21-26] using electro paramagnetic resonance (EPR) method based on the number of counted stable radiation induced radicals [10]. On the other hand, tooth enamel is a kind of TL retrospective dosimetry and possibly a useful alternative way to EPR retrospective dosimetry meanwhile it needs substantially lesser amounts of sample (only few mg) that may be harmlessly gotten by dentists without tooth removal [11]. A few researchers [10, 12-16] have investigated the thermoluminescence properties of two major inorganic minerals which are hydroxyapatite and fluorapatite. Alvarez et al. [27] carried out the thermoluminescent characteristics of synthetic hydroxyapatite which is one of the most important ingredient in tooth enamel. Two main peaks centered around 200°C and 300°C are seen and good TL properties such as wide linearity range and good reproducibility is observed.

In the current study, the thermoluminescence (TL) intensity-dose response relation of fluorapatite mineral which is one of the important minerals in tooth enamel under the different annealing temperatures were investigated and then analyzed its thermoluminescence glow curve peaks.

This thesis consists of five main chapters. In chapter 1, the importance of the thesis and previous studies about TL properties of the minerals in tooth enamel are shortly mentioned.

In chapter 2, theory of the thermoluminescence (TL), the structure of a tooth, the histology and the morphogenesis of tooth enamel, its mineral phase have been given.

In chapter 3, experimental procedure of the studies, the crystalline structure of the sample and equipments which are used in experiments are have been introduced.

In chapter 4, all graphs obtained from experiments and the analyses of their results are mentioned.

In the last chapter of the thesis, chapter 5, the discussion and conclusion of the study have been summarized.



## CHAPTER 2

### LITERATURE SURVEY

#### 2.1 Tooth structure

The tooth consist of two anatomical parts. These two parts are crown and root.

The crown of the tooth is a part of a tooth which is covered with enamel and usually seen in the mouth. The crown is found above the gingiva and can have several shapes, subjected on the type of tooth. Eventually, it can undergo significant changes; abrasion, elongation, erosion or dental decay that causes demineralization and annihilation of the rigid tissues of the tooth crown.

The root is the part of the embedded part in the jaw. It attaches the tooth in its bony socket and is generally not visible. The root is devoted to the jawbone by a group of particular connective tissue fibers called the periodontal ligament. A tooth may have one or more roots. Usually, front teeth have a sole root though molars can have two, three or more roots but this differs from individual to individual. [28]

This study is planned to ensure elementary data required for using tooth enamel dosimetry. For this reason, caution will be focused largely on morphogenesis and histology of tooth enamel.

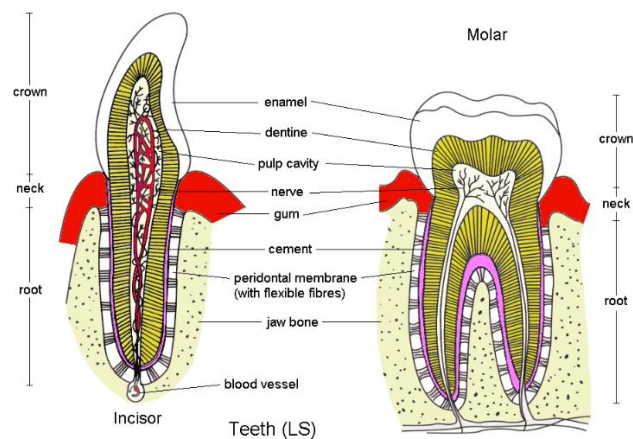


**Figure 2.1.** Tooth structure, parts of teeth

## 2.2 Tooth Enamel

### 2.2.1 Histology of Tooth Enamel

The histological construction of tooth enamel is shaped by mineral crystallites of hydroxyapatite grouped in clusters with hexagonal cross-sections. It is created by millions of enamel prisms or rods, which run from the amelo-dentinal junction to the tooth enamel surface. Each prism consists of a lot of tooth enamel crystallites.

Tooth enamel is made of ~% 96 inorganic minerals by weight, the basic inorganic constituent being hydroxyapatite, % 1 organic mineral by weight and the basic organic constituent being protein and % 2-3 water by weight.

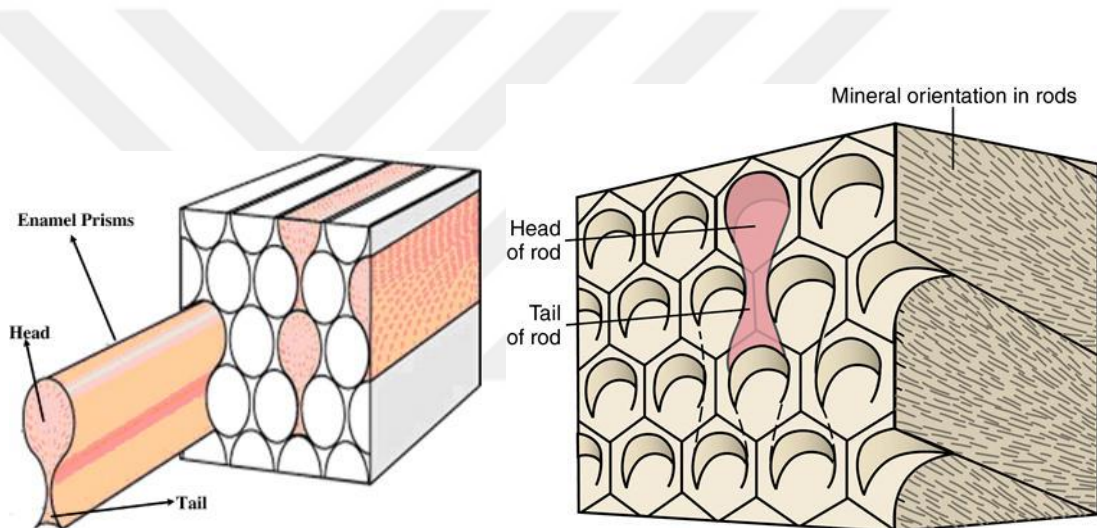


**Figure 2.2** Structure of tooth enamel

### 2.2.2 Tooth Enamel Morphogenesis

Tooth enamel mineral is mainly shaped at the dentin-enamel junction. When the crystals have nucleated, they elongate in the direction perpendicular to the junction to form the mentioned rods.

Cells that hide enamel crystals are called ameloblasts. Ameloblasts are acquired from oral epithelium tissue of ectodermal origin. Their distinction from preameloblasts, whose origin is from inner enamel epithelium, is a consequence of signaling from the ectomesenchymal cells of the dental papilla. Ameloblasts are cells which hide the enamel proteins enamelin and amelogenin which will later mineralize to form enamel, the solidest material in the human body. Ameloblasts control ionic and organic structures of enamel.

Apatite is the most common phosphate mineral. The teeth of most creatures are consist of calcium phosphate, which is the identical mineral as apatite. These biological apatites are nearly solely the Hydroxylapatite type. Formation of apatite crystals can be considered in three stages. These stages are; secretion stage, transition and maturation period.

The secretory stage fundamentally includes the secretion of matrix and the preliminary mineral phase and can be considered whole when full thickness of the tissue has been laid down [29].

This is followed by a maturation period throughout which final matrix exclusion occurs and final mineral content is obtained. Final mineralization is probable finalized post eruption, a phase not conciliate by cells of the enamel organ [30, 31].

Between secretion and maturation there is a so called transition period [32, 32]. Since this looks to arise at or after major amelogenin secretion, it is involved here principally as a primary phase of maturation. Many variations characteristic of maturation begin in transition and happen across the boundary between transition and maturation proper.

Maturation stage; is characterized by the conclusion of calcification. Solid tissues including enamel and dentin grow during this period. Formation of dentin, known as dentinogenesis, is the first identifiable feature of this stage. The creation of dentin must permanently happen before the creation of enamel. The diverse periods of creation of

dentin results in different types of dentin: mantle dentin, primary dentin, secondary dentin and tertiary dentin.

### **2.2.3 Mineral Phase**

The main mineral constituent of hard tissue is hydroxyapatite such as human teeth. Replacements within the hydroxyapatite lattice are detected both for naturally happening and synthetic hydroxyapatite. The most mutual substitutions are including carbonate, fluoride and chloride ions for hydroxyl ions [34]. The mineral phase of tooth enamel contains apatite including 0.04wt% to 0.07wt% of fluoride, and 95% to 97% of the dry mass[35].

### **2.3 Thermally Stimulated Luminescence (TL)**

Thermally stimulated luminescence has been used comprehensively to evaluate radiation doses since the early 1950s [37] subsequent the marketable availability of adequately sensitive and admissible photomultiplier tubes. Thermoluminescence was consequently applied to archaeological dating in 1960s [38-40] and applied to geological dating in the earlier stages of the 1980s [41] Aitken examined the techniques and methods used in TL dating[39]. Heating a material at a constant rate to the finite temperature is usually analyzed (e.g. 500°C) and recording the luminescence emission versus temperature on the part of thermoluminescence. The TL output is described by a TL glow curve, with distinguishable peaks arising from at diverse temperatures, which associate to the electron traps existing in the material. The lattice structure imperfections are responsible for these traps.

The dislocation of a negative ion may create the characteristic defect, providing a negative ion vacancy that behaves like an electron trap. For this once trapped, thermal vibrations of the lattice will ultimately discharge an electron. When the temperature is increased, these vibrations become stronger, and the probability of dislodgement rises so quickly that inside a narrow temperature region trapped electrons are rapidly released. Some electrons then give rise radiative recombination with trapped holes, consequential in emission of light. A characteristic TL glow curve derived from sedimentary feldspar is shown in Figure 2.3. Different electron trap depths to the temperature peaks are clearly seen.



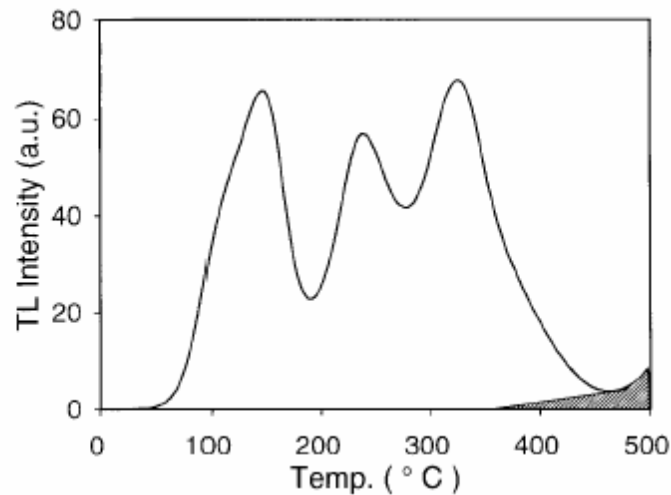


**Figure 2.3** Typical thermoluminescence glow curve from a sedimentary K-feldspar sample given a beta dose of 8 Gy in addition to the natural dose (approximately 200 Gy). The 150°C peak evident in this figure has been created by the recent beta dose; it is not usually evident in the natural signal as it has normally decayed away. The shaded area is the lack body radiation observed when the sample is heated a second time with no additional irradiation [36].

Nevertheless, a thermoluminescence glow curve can appear to be a flat continuum, it is comprised of a number of imbrication peaks obtained from the thermal discharge of electrons from traps of different determinations. Electrons in superficial traps is shorter than that of the lifetime of electrons in deep traps. Usually, for the use of dosimetry, traps generate to glow curve peaks lesser than 200 °C are not useful as electrons may be flowed from these traps over an extended time even at environmental temperatures. Unchanging glow peaks favorable for dosimeter normally take place at 300°C or bigger. In addition to this, unexpected evanescing of high temperature glow peaks at room temperature has been founded in some feldspars. This may be clarified as a tunneling effect [42]. Alternative confusion in thermoluminescence measurements is thermal quenching. Some peaks found in high temperature region in quartz and feldspars are expose to thermal quenching pro processes, for example, the bigger probability of non-radiative recombination at high temperatures [43].

## 2.4 Dose Response

Dose response  $F(D)$  is a functional relation between the thermoluminescence intensity and the absorbed radiation dose. This relation would be expected linear over a wide dose range for a good dosimeter. But, most dosimetric sample used in practical dosimeter demonstrate a diversity of non-linear effects, as shown in Figure 2.4. Especially, once finds that the response of a TLD material is linear, in that case sublinear as the dose is increased. We describe that the normalized dose response function  $f(D)$ :

$$f(D) = \frac{\left(\frac{F(D)}{D}\right)}{\left(\frac{F(D_1)}{D_1}\right)} \quad (2.1)$$

where  $F(D)$  is the dose response for a dose  $D$ , a low dose at which the region becomes linear is defined as  $D_1$ . Thus, when over a wide dose range, the ideal dosimeter should satisfy  $f(D) = 1$ , say  $D$  varies from 0 Gy to MGy. Unluckily, in many TLD materials,  $f(D) = 1$  is found only over a small dose region, up to a few Gy. Supralinearity, known as  $f(D) > 1$ , is prevalently observed, during the approximate to saturation, sublinearity, known as  $f(D) < 1$ , is most often observed. Linearity, supralinearity and sublinearity characteristics are shown in examples of growth curves for three different TLD materials are illustrated in Figure 2.4. Nonlinearity is not essentially a somber problem so long as the nonlinear characteristic is single valued and a dependable correction curve can be created.

The real value of  $f(D)$  for the given dose depends on type of sample, some external parameters, the type and energy of the radiation source, and the all procedure during heating the sample to get glow curve. And also the  $f(D)$  depends upon the linear energy transfer or ionization density of the radiation area. For instance,  $f(D)$  values, gotten at about 0.2 kGy, for LiF TLD-100 have been calculated as big as  $\sim 3.5$  for  $^{60}\text{Co}$  irradiation, but only  $\sim 1.5$  for 20 kV<sub>p</sub> X ray irradiation [44-46], and  $\sim 1.0$  for alpha particle irradiation [47,48]. Not only is the degree of the supralinearity reliant on LET, but the dose at which the beginning of supralinearity becomes obvious is also LET-dependent [47,49], and even the spectra can alter [50].

The nature of the host sample defines the parameters of the most known dosimetric samples itself. For instance, in Figure 2.4 we see that the growth of TL with dose in

quartz sample is extremely supralinear that means  $f(D) > 2$  seen in curve A whereas for  $\text{CaF}_2:\text{Mn}$  it is nearly linear that means  $f(D) = 1$  seen in curve C.  $\text{LiF}:\text{Mg},\text{Ti}$ , though, shows a linear, supralinear and sublinear response seen in curve B.

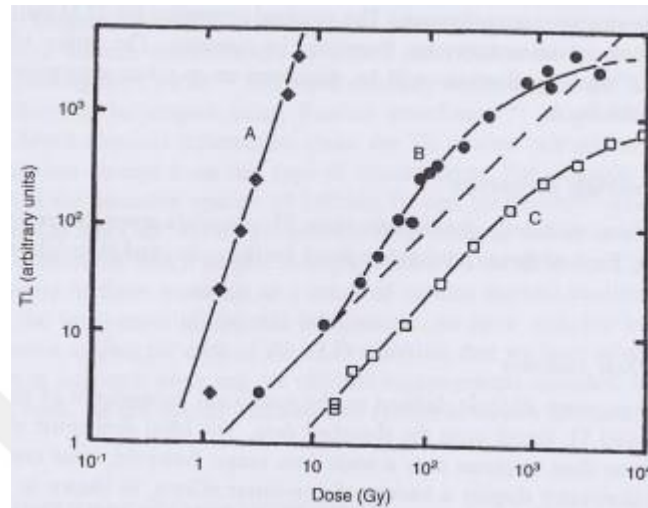


**Figure 2.4** Examples of growth curves for three thermoluminescence samples. Curve A: The thermoluminescence dose response for the 100 °C peak in  $\text{SiO}_2$ . Curve B: The dose response is linear, supralinear and sublinear for peak 5 from TLD-100 ( $\text{LiF}:\text{Mg},\text{Ti}$ ). Curve C: The dose response of TLD-400 ( $\text{CaF}_2:\text{Mn}$ ) in which supralinearity is very weak. The linear dose response is indicated by the dashed line.

Furthermore, in  $\text{SiO}_2$  the supralinear behaviors can be completely removed by suitable annealing processes [51]. In  $\text{LiF}:\text{Mg},\text{Ti}$ , falling the Mg content improves supralinearity [49], while rising the OH impurity content declines supralinearity [50,51] Shortly, the nature of the host material and its defect structure identify the dose response of the materials.

There are a lot of theories to understand the reasons of supralinearity in thermoluminescence dosimetric materials materials-particularly  $\text{LiF}:\text{Mg}$  type materials (e.g. TLD-100). Suitably, they are classified as models in which the serious procedures happen during the absorption of radiation, and models in which the serious procedures happen during heating (i.e. during TL readout). (For detailed discussions and criticisms of all the relevant models see publications by McKeever[48,52,53] and by Horowitz[54,55].) The proof, at minimum for  $\text{LiF}$ -based samples, obviously gives

that the most important mechanism is that of competition during the heating part of TL readout. During heating process, electrons escaped from electron traps, can probably either recombine with holes in recombination center to yield thermoluminescence light or be retrapped in deeper traps, which act as competing centres. At low dose values, where the distance between traps and recombination sites is big, the chance that a freed charge may meet with a recombination site without dropping into a competing trap is low. Thus, the response of the dosimeter is reduced in this low dose region. This is indicated in Figure 2.5(a), curve A. At bigger doses, however, not only is the mean distance between traps and recombination centers reduced, but the number of competing sites is also reduced. (It should be realized that a competing trap is an empty trap; once filled, it no longer acts as a competitor.) Thus, at higher doses the response of the dosimeter is enhanced and more TL per unit dose is the result. Finally, at very big doses, the sample saturates. Such a sample has  $f(D) > 1$  over the whole dose region, up to saturation; an example is  $\text{SiO}_2$ , shown in Figure 2.4.

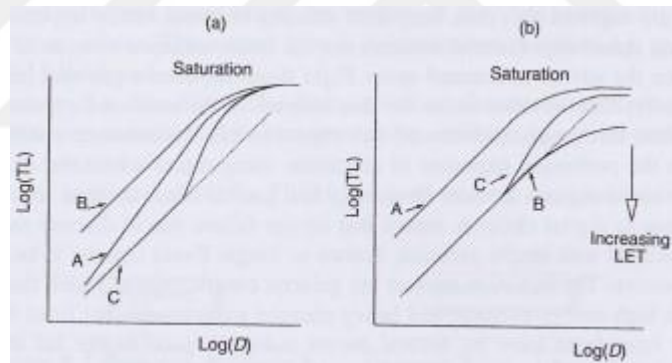


**Figure 2.5** Schematic dose response curves for several cases. Note that this is a log-log plot in which  $f(D) = 1$  is indicated by a slope of 1 (viz. the dashed line). (a) High energy photon irradiation: Curve A, supralinear growth due to competition during heating. With an isotropic distribution of traps, competing traps and recombination sites, the dose response curve is supralinear ( $f(D) > 1$ ) from the lowest doses, up to saturation ( $f(D) < 1$ ). Curve B, an absence of competition results in more TL per unit dose at low doses and a linear response ( $f(D) = 1$ ). Curve C, spatial association of traps and recombination centres lead to an initial linear region before the onset of supralinearity. All three curves are shown with the same saturation region, for simplicity. The dashed line is to guide the eye and represents a slope (on the log-log plot) of 1, i.e.  $f(D) = 1$  (linearity). (b) HCP irradiation: Curve A, the dose response

curve for low LET irradiation without competitors. This is equivalent to curve B of part (a). Curve B, the dose response of high LET particles. The dose response is again linear since the high ionization density ensures that, within the track, there is a lack of competitors and recombination of all trapped charges. The saturation level is low. Curve C, dose response for the intermediate case, with competitors. Successful interaction between tracks occurs when the inter-track distance is low enough, causing supralinearity and an intermediate saturation level.

If the material did not have any competing traps (no competition), the sensitivity (i.e. TL per unit dose) would be higher at low doses and linearity would be observed up to saturation (curve B, Figure 2.5(a); an example is  $\text{CaF}_2:\text{Mn}$ , shown in Figure 2.4). Thus we see that supralinearity should correctly be considered to be an under-response at low doses, rather than an over-response at high doses.

The competition-during-heating process was first suggested by Rodine and Land[56] and was later analysed mathematically by Kristianpoller et al[57] (using a kinetic analyses of retrapping and recombination) and by Mische and McKeever[49] (using probability analysis). The prediction from these analyses is that this mechanism produces a dose response curve which is supra linear from the lowest dose, all the way up to the saturation region (viz. curve A in Figure 2.5(a)). However, as observed with several TLD dosimeters, one often finds a linear region before the supralinear region (see  $\text{LiF}:\text{Mg},\text{Ti}$  in Figure 2.4 and curve C in Figure 2.5(a)). To explain this it is necessary to invoke spatial localization between the traps and the recombination centres. This type of effect is typified by  $\text{LiF}:\text{Mg},\text{Ti}$  phosphors in which the traps- believed to be  $\text{Mg}-\text{Li}_{\text{vac}}$  complexes-are closely associated with the recombination sites- believed to be  $\text{Ti}-\text{OH}$  complexes. (More detail regarding the defects responsible for the TL in this material can be found in Chapter 3). As demonstrated by Mische and McKeever[49], spatial association of this type produces a linear term at low doses, before one observes the non-linear effect at higher doses. All three types of dose response curve are illustrated schematically in Figure 2.5(a).

An important feature of the analysis described by Mische and McKeever[49] is the spatial distribution of the trap-recombination centre pairs with respect to each other. With high energy gamma (low LET) one may safely view the distribution of such sites as an “isotropic sea”. However, for heavy charged particle(HCP) irradiation with high

LET, we have a non-isotropic distribution of densely ionized region along linear tracks. Calculations by Butts and Katz[58] and Kalef-Ezra and Horowitz[59] indicate that the dose is deposited within a few tens of nanometers of the track centre for high LET particles and that the tracks have approximately cylindrical geometry. Thus, we can imagine regions within the track of high concentrations of trapped charges and very few competitors, and regions between the tracks of very few trapped charges and high numbers of competitors. For high ionization densities the mean free path of the freed electron inside the track is less than the track radius and recombination within the track, leading to TL, is highly probable. Thus, the dose response curve is linear, although it saturates early since all the available sites within the track volume become quickly saturated (Figure 2.5(b), curve B). For lower LET particles, there is a probability that some electrons will escape from the track core without recombining and thus enter the inter-track region. Here the probability of finding a competitor is high and the electron is likely to be lost from the TL process. However, as the dose is increased the probability of reaching an adjacent track also increases since the inter-track distance decreases. The escaped electron may now recombine with a hole in an adjacent track and so produce a TL photon. Under these circumstances, the TL output (per unit dose) will also increase and thus supralinearity (Figure 2.5(b), curve C). It is clear that as the LET of the HCP increases, the tracks become more localized and consequently the dose levels at which track interaction can take place also increase. In this way this mechanism can easily encompass the observed LET-dependence of the value of  $f(D)$ , and of the dose at which the onset of the supralinearity occurs. The process described is known as track interaction and has been studied extensively by Moscovitch and Horowitz[47]. The effect on the dose response curves is depicted schematically in Figure 2.5(b).

An additional property required of a TLD material is that its dose response should be independent of the rate of irradiation. Measurements at extremely high dose rates using pulsed X ray sources have revealed this to be the case for several common TLD materials. Fortunately, dose rate dependence does not seem to be a problem for most materials.

## 2.5 Annealing

Annealing is the thermal process desired to delete any dose from the dosimetric sample. The annealing at higher temperature is essential to erase the unwanted accumulated dose which can induce undesired background through following usage of the dosimeters. The annealing at lower temperature is done to make steady and accumulate traps emptied at lower temperature with the purpose of improve the sensitivity of the main dosimetric traps and to decrease signal losses by radiation effect because of thermally or optically fading. The mixture of these two annealing processes is named standard anneal [60].

To use a thermoluminescent sample for dosimetric purposes, the sample must be prepared. At first, all the dose from any prior process must be deleted from it, i.e., the initial conditions of the crystal should be supplied for each reading. It is aimed to supply stability of the trap.

With the purpose of preparing a thermoluminescent sample, it is wanted to accomplish a thermal treatment, usually called annealing [61,62].

In the first usage of a new TL material, the annealing process is necessary to perform. The annealing treatment has three essential goals. Firstly, it is to delete any remaining dose from preceding irradiation. Secondly, it is to reset the sensitivity to a known value. Thirdly, it is to reduce fading of the stored signal after irradiation (i.e. post irradiation anneal).

There are two basic ways of annealing. One of them, reader anneals usually for low dose measurements, e.g. less than a few cGy and another, external anneal for high doses or long intervals before irradiation and readout.

Different annealing temperatures and times for a TL material may change the TL properties of the material. For this reason, they change the shape of the glow curve during readout after irradiation.

The cooling rate immediately after annealing may also affect the response (light output) of TL materials. Some TL materials e.g. LiF:Mg,Ti are very much affected by the annealing and cooling rate while others may not be affected at all. Hence, for TL

materials like LiF:Mg,Ti a fixed annealing and cooling regime should be applied in order to achieve consistent and accurate results.

The annealing processes normally done for the TLDs can be classified into three branches:

**Initialisation Treatments:** This process is done for unused thermoluminescence materials or for dosimeters which have not been used for a long time. The purpose of this annealing is to make stable the trap's positions, thus that during following uses the basic background and the sensitivity are both reproducible. The standard annealing normally includes both time and temperature of the initialization annealing.

**Erasing Treatment or Standard Annealing (Pre-irradiation Annealing or Post-readout Annealing):** This process is done for erasing any prior remaining irradiation effect. It is performed before measurements. The main aim of these annealing process is to restore the defects structures to the former one obtained after the initialization procedure. It may consist of one or two annealing process.

**Post-irradiation or Pre-readout Annealing:** This type of annealing is used to delete the peaks located in the lower temperature region. This kind of peaks is generally subjected to a rapid thermal decay (fading) and perhaps has not to be involved in the reading to eliminate mistakes in the dose evaluation.

The cooling rate after the annealing has big importance for the performance of a thermoluminescence dosimetric system. The fast cooling causes enhancement in TLD sensitivity. The maximum sensitivity is observed when a cooling rate is 50-100 °C/s. For the fast cooling, the TL sample must be placed directly on a cold metal block after the annealing. The process must be repeatable and unaffected from all conditions during the whole use of the dosimeters.

It has to be mentioned that the thermal processes given above may be studied in the TLD reader. This can play an important role for thermoluminescence materials placed in plastic cards as the dosimeters used for big personnel dosimetry services. Unfortunately, the plastic cards may not be able to eliminate higher temperatures and the in-reader annealing is not enough to anneal sample. But, its efficiency is very low when the dose value is high. This process can only be applied if the dose value is smaller than 10 to 20 mGy. Driscoll [61] proposes an extra annealing in furnace about



20 hours at 80 °C for cards holding LiF:Mg,Ti; at this temperature the plastic holder does not suffer any deformation. For TL solid chips or TL materials in powder forms without plastic card, the annealing can be done in an furnace.



## CHAPTER 3

### EXPERIMENTAL PROCEDURE

In this chapter, the structure of the sample and equipments used in the experiments and also experimental procedures are given.

#### 3.1 Material

The tooth enamel samples were procured from a dentist who separated enamel from dentine. The samples were crushed in the agate mortar to get powder form. The powdered tooth enamel sample was etched for 5min in a 20% acetic acid water solution followed by drying [63]. Each experiment was performed with 10 mg aliquot samples. The sample of the tooth enamel and its powder form used in this study are shown in Figure 3.1 and 3.2.



**Figure 3.1** Sample of the tooth enamel.



**Figure 3.2** The powder tooth enamel sample

The x-ray diffraction (XRD) pattern and Peak ID Extended Report of tooth enamel were performed by a Rigaku D/MAX-Ultima+/PC X-ray diffraction equipment from XRD Facility of Bogaziçi University Advanced Technologies R&D Center, are shown in figure 3.3 and table 3.1. The Rigaku D/MAX-Ultima+/PC X-ray diffraction equipment is engineered to create a multiple purpose configuration. The x-ray generator is a part of Rigaku D/MAX-Ultima+/PC X-ray diffraction equipment and operates at 20kV-60kV rated voltage, 2 mA -80mA rated current and 3kW maximum rated output with SCR phase control. The focal spot size in the x-ray generator is  $1 \times 10 \text{mm}^2$ [64].

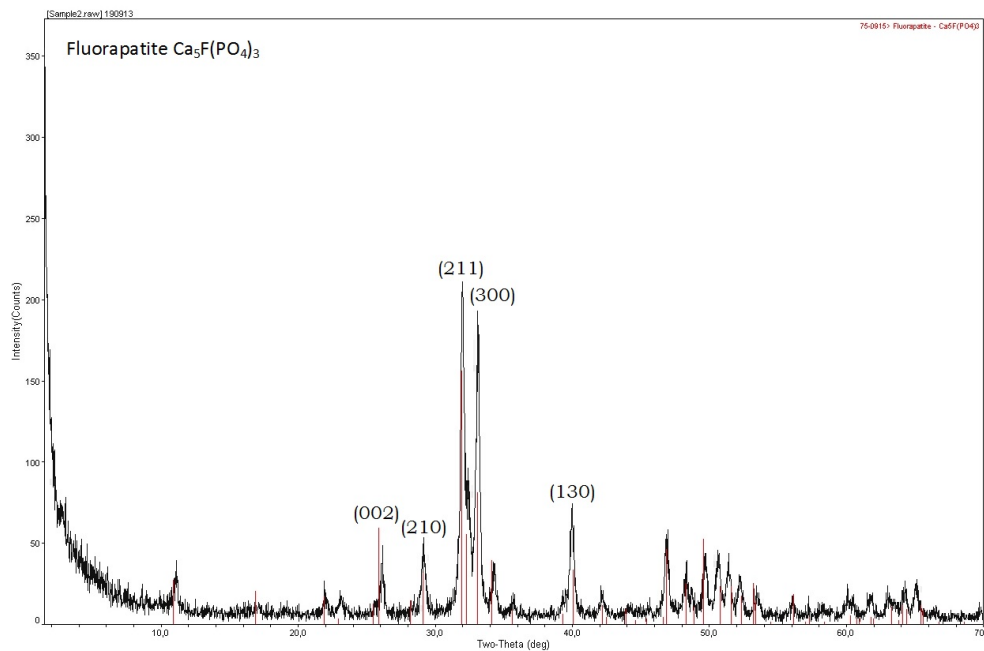


**Fig. 3.3** X-ray diffraction (XRD) pattern of tooth enamel

**Table 3.1** The Peak ID Extended Report of tooth enamel.

2 $\theta$	d(Å)	Height %	Phase ID	hkl
26,175	3,4018	21,5	Fluorapatite	( 0 0 2)
29,177	3,0582	23,5	Fluorapatite	( 2 1 0)
32,019	2,7929	100,0	Fluorapatite	( 2 1 1)
33,122	2,7024	92,0	Fluorapatite	( 3 0 0)
40,035	2,2503	34,5	Fluorapatite	( 1 3 0)

## 3.2 Equipments

### 3.2.1 Radiation Source and Irradiator

The  $^{90}\text{Sr} - ^{90}\text{Y}$  point  $\beta$ -source which delivers 0.040 Gy/s is used to irradiate the samples. The activity of beta source was about 100 mCi. Its calibration date is on March, 10, 1994.

Strontium-90 ( $^{90}\text{Sr}$ ) emits high energy beta particles. Beta radiation is absorbed by air, so its intensity reduced with distance much more fastly than inverse square law calculations would designate. The maximum range of Yttrium-90 ( $^{90}\text{Y}$ ) beta particles in air is roughly 9 meter. The irradiation instrument is an insertion part of the 9010 Optical Dating System which is bought from Little More Scientific Engineering, UK. The irradiation source instrument interfaced to PC computer using a serial RS-232 port[65].



**Figure 3.4** Radiation source installed in a 9010 optical dating system which is interfaced to a PC using a serial RS-232 port.

### 3.2.2 TLD Reader

The Model 3500 TLD reader shown in Figure 3.5 has been used to read the irradiated samples and obtain the glow curves for each sample. The instrument includes a sample change drawer for inserting and removing the TLD sample, a thermoelectrically cooled photomultiplier tube with associated data acquisition circuits for reading the light emitted by the TLD sample. The TLD reader has a heating system which linearly increases the ambient temperature. A separate computer with application software performs all other functions, including user interface, acquisition, and storage and retrieval of TLD data [66]. Signal acquisition and conditioning are performed in the reader. The program resolves the individual peak present in the curve, giving the best values for the different peak parameters. All processes in TLD reading are indicated in Figure 3.6.



**Figure 3.5** TLD Reader

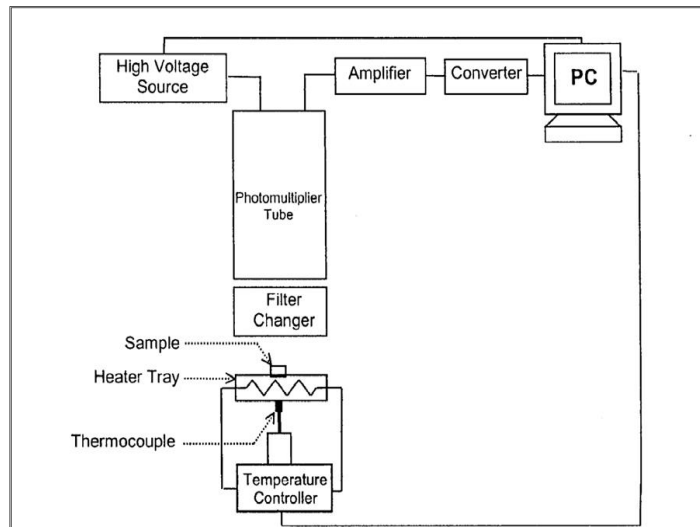


**Figure 3.6** Basic block diagram of TLD reader.

### 3.2.3 Annealing Furnace

A microprocessor controlled furnace whose temperature range varies from room temperature to 1100 °C was used to perform thermal treatments. This equipment shown in Figure 3.7.



**Figure 3.7** Annealing Oven

### 3.2.4. Digital Balance

A digital balance is used to estimate the weight of the used sample and shown in Figure 3.8.



**Figure 3.8** Digital Balance

### 3.2.5. Mortar

A mortar made by agate is used to crush the tooth enamel samples and to get powder form given in Figure 3.9.



**Figure 3.9** Agate Mortar

### 3.3. Experimental Procedure

The prepared tooth enamel sample weighed about 10 mg was firstly annealed at 400 °C about 30 minutes in a microprocessor controlled furnace. Then, the annealed

sample was irradiated 154 Gy by using  $^{90}\text{Sr} - ^{90}\text{Y}$  point  $\beta$ -source and read out from 30°C to 400°C in 1°C per second increments by Harshaw 3500 TLD Reader. This process is done for five different radiation dose values (from 154 Gy to 2.46 kGy). The process mentioned above is repeated for different annealing temperatures (400 °C, 500 °C, 600 °C, 700 °C, 800 °C, 900 °C, 1000 °C and 1100 °C)





## CHAPTER 4

### EXPERIMENTAL RESULTS AND DISCUSSIONS

In this thesis, thermoluminescence (TL) intensity-dose response relation of fluorapatite mineral in tooth enamel under the different annealing temperatures were investigated and then analyzed its thermoluminescence glow curve peaks with a computer programs.

#### 4.1 Glow Curve Variations

In this part of the experiments, the glow curves of sample were observed by using different doses. We aimed to see the variation of glow curve shape with increasing annealing temperature.

#### 4.1.1 The Glow Curve Variation of Sample Annealed at 400 °C

In Figure 4.1, variation of shape of glow curves of the sample annealed at 400 °C as a function of applied dose was examined. The shape of glow curves do not change by using different doses. There are no extra peaks. There is one wider peak located around 220°C.

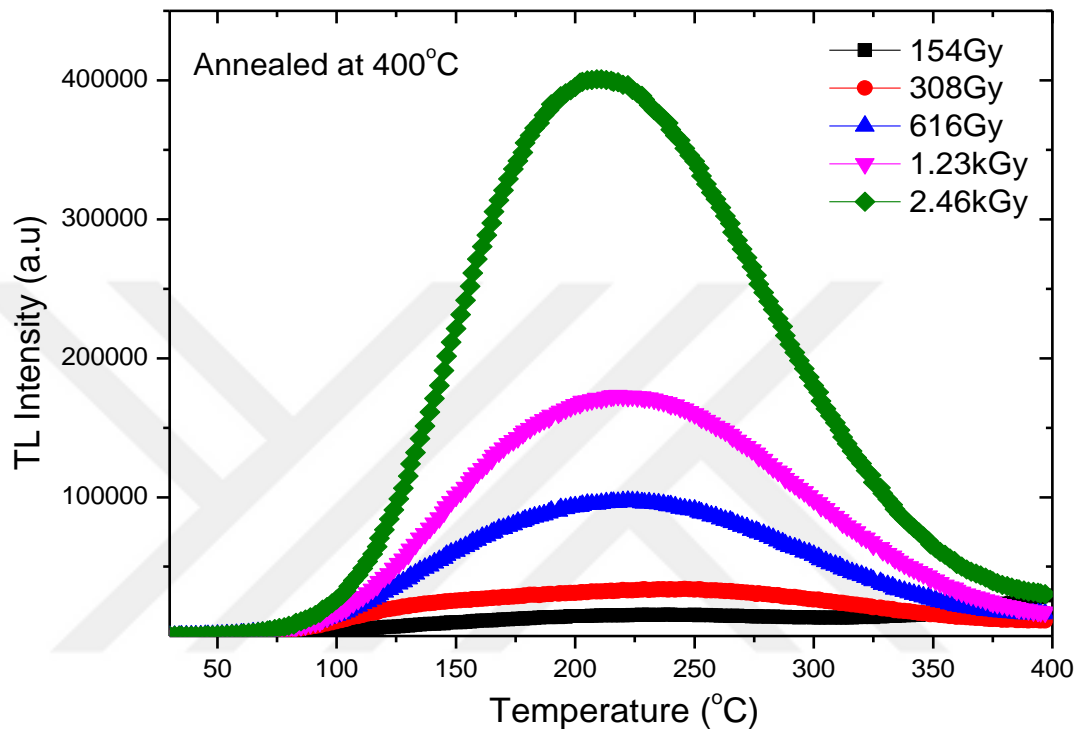


**Figure 4.1** Variations of shape of glow curves of the sample annealed at 400°C as a function of applied dose.

#### 4.1.2 The Glow Curve Variation of Sample Annealed at 500 °C

In Figure 4.2, variation of shape of glow curve of the sample annealed at 500 °C as a function of applied dose were examined. We observed that, doses at 154 Gy to 616 Gy, the glow curve shapes are different from each other. A reason may be the alteration of trap position in the sample. In doses 1.23 kGy and 2.46 kGy, glow curve shapes are the same, but extra peaks may be occurred in 250-400 °C temperature region. At 154 Gy, the wider peak is located around 150 °C, but the wider peak is located around nearly 220 °C in doses between 308 Gy and 2.46 kGy.

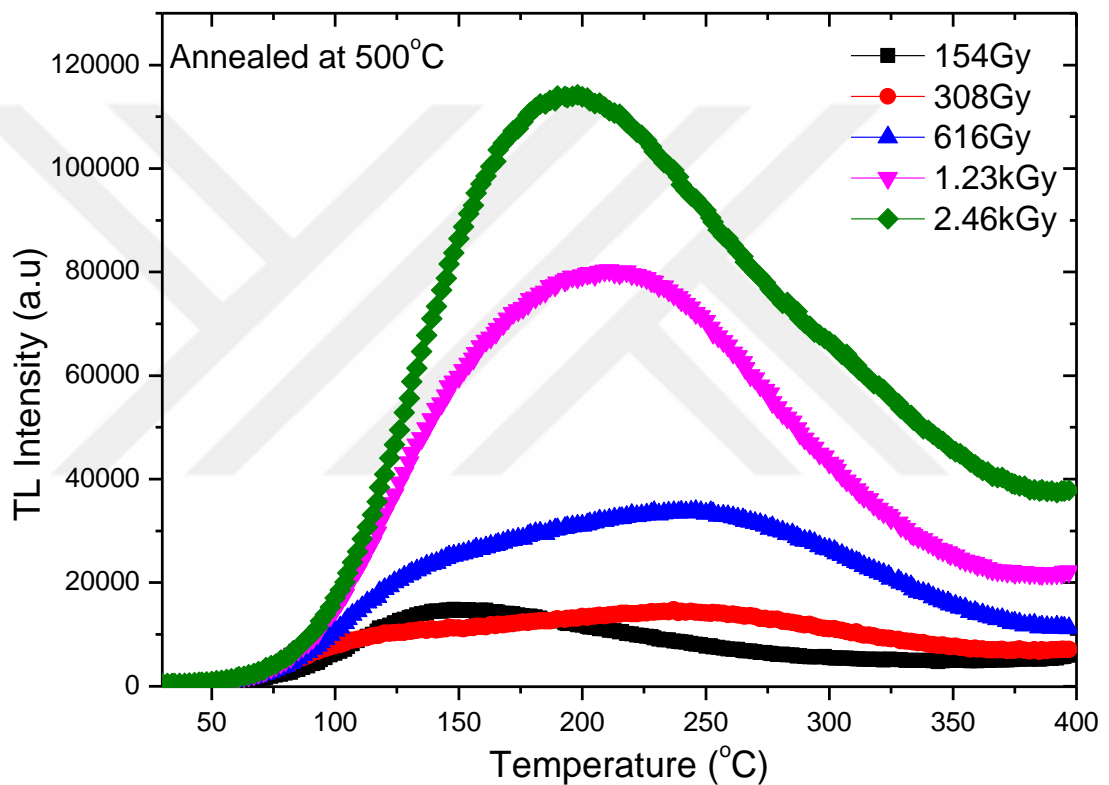


**Figure 4.2** Variations of shape of glow curves of the sample annealed at 500 °C as a function of applied dose

### 4.1.3 The Glow Curve Variation of Sample Annealed at 600 °C

In Figure 4.3, variations of shape of glow curves of the sample annealed at 600 °C as a function of applied dose were examined. We observed that, peaks are not increased in same proportion from 154 Gy to 308 Gy. But doses at 616 Gy to 2.46 kGy, peaks increase nearly the same proportion. For doses between 154 Gy and 308 Gy, the wider peak is located around the right side. And also, no variation in the shape of glow curve is observed except 154 Gy and 308 Gy dose levels.

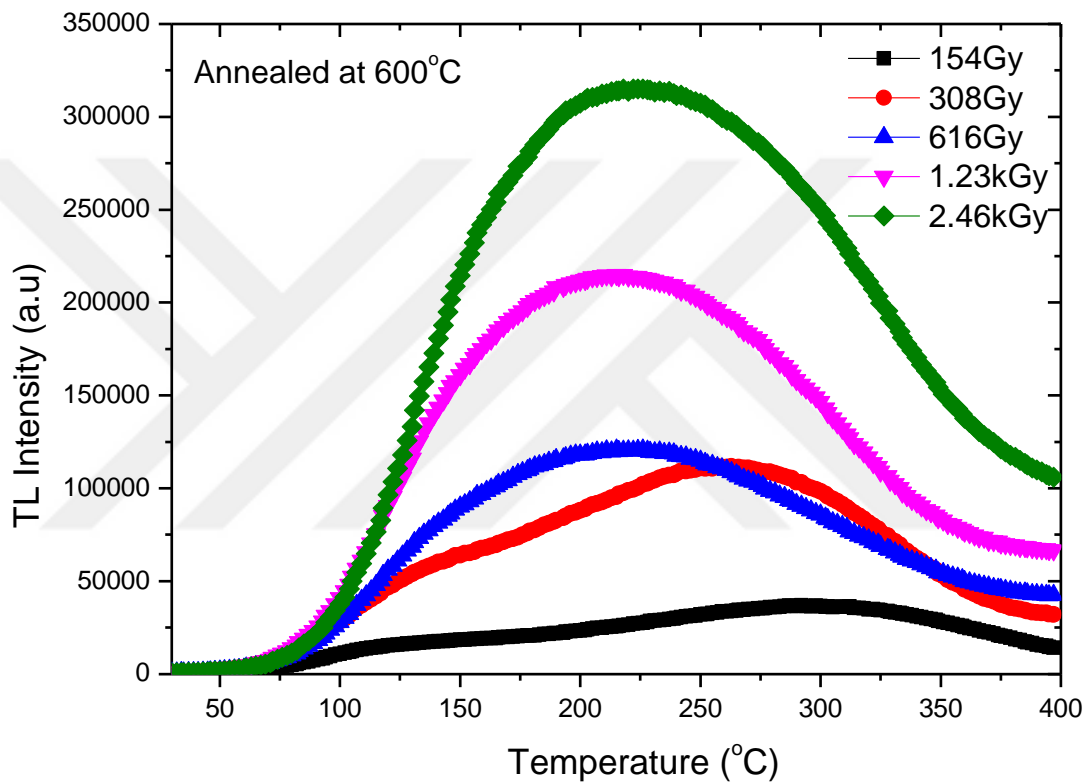


**Figure 4.3** Variations of shape of glow curves of the sample annealed at 600 °C as a function of applied dose

#### 4.1.4 The Glow Curve Variation of Sample Annealed at 700 °C

In Figure 4.4, variation of shape of glow curves of the sample annealed at 700 °C as a function of applied dose were examined. The shape of glow curves do not change by using different doses. Also, peaks are increase the same proportion.

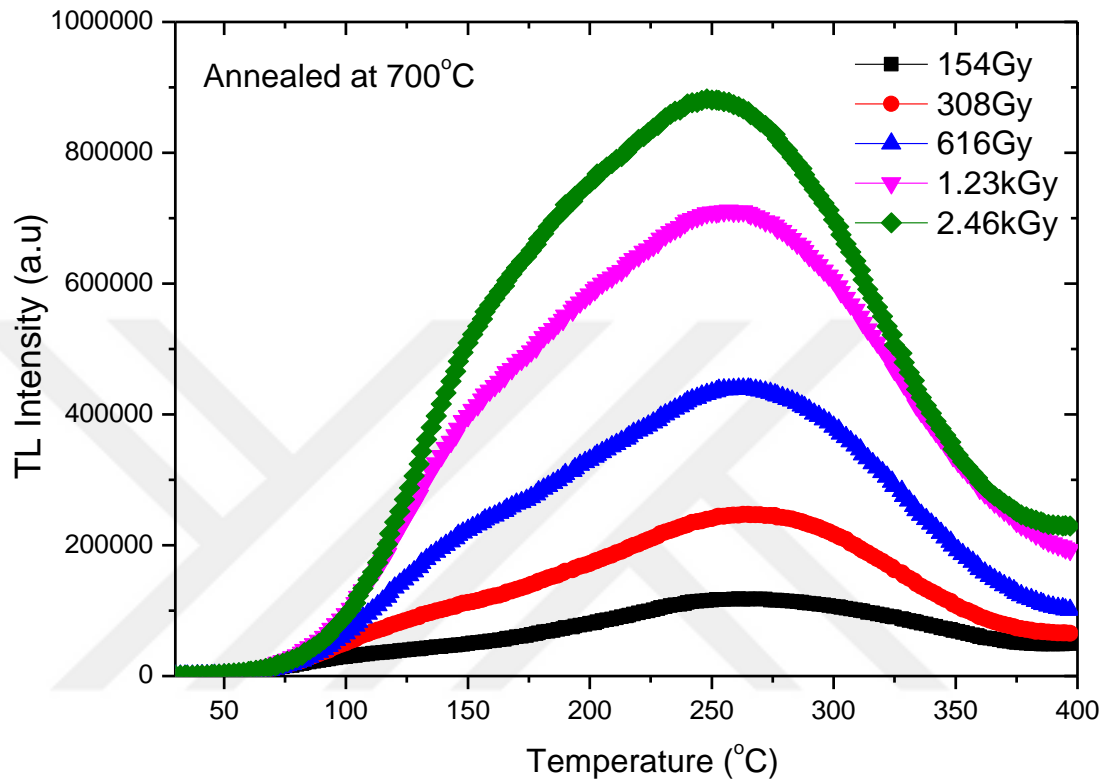


**Figure 4.4** Variation of shape of glow curves of the sample annealed at 700 °C as a function of applied dose

#### 4.1.5 The Glow Curve Variation of Sample Annealed at 800 °C

In Figure 4.5, variation of shape of glow curves of the sample annealed at 800 °C as a function of applied dose were examined. The shape of glow curves do not change by using different doses.

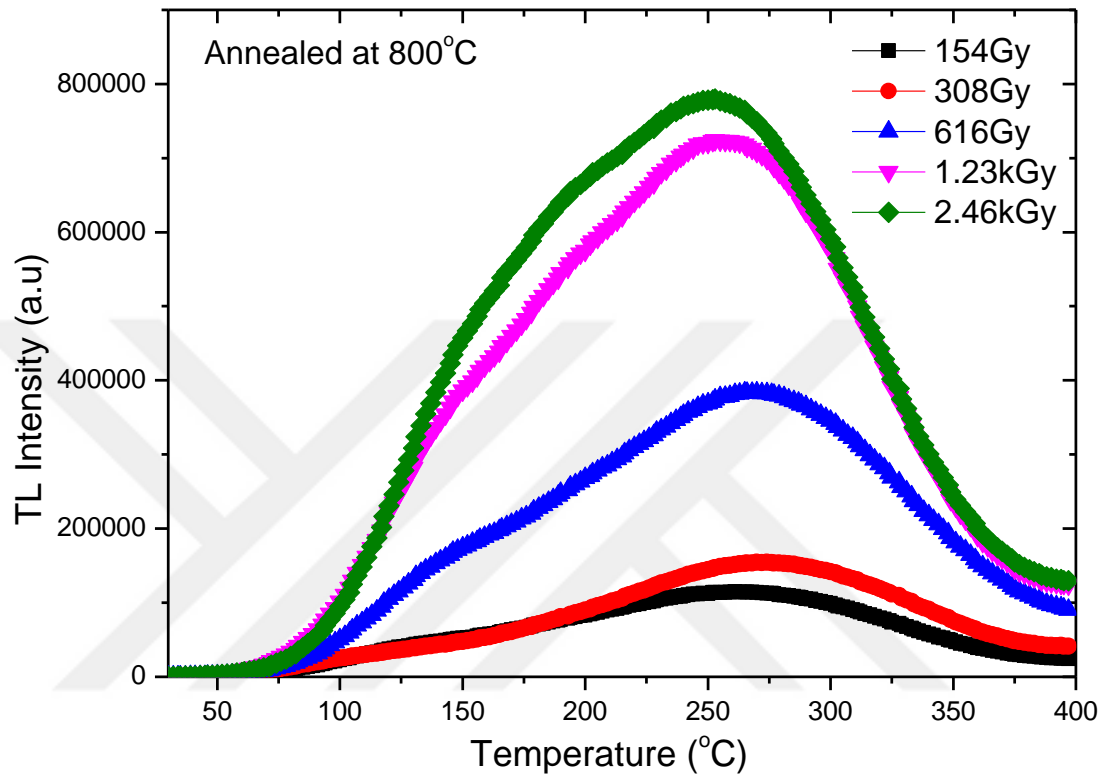


**Figure 4.5** Variations of shape of glow curves of the sample annealed at 800 °C as a function of applied dose

#### 4.1.6 The Glow Curve Variations of Sample Annealed at 900 °C

In Figure 4.6, variations of shape of glow curves of the sample annealed at 900 °C as a function of applied dose were examined. The shape of glow curves do not change by using different doses.

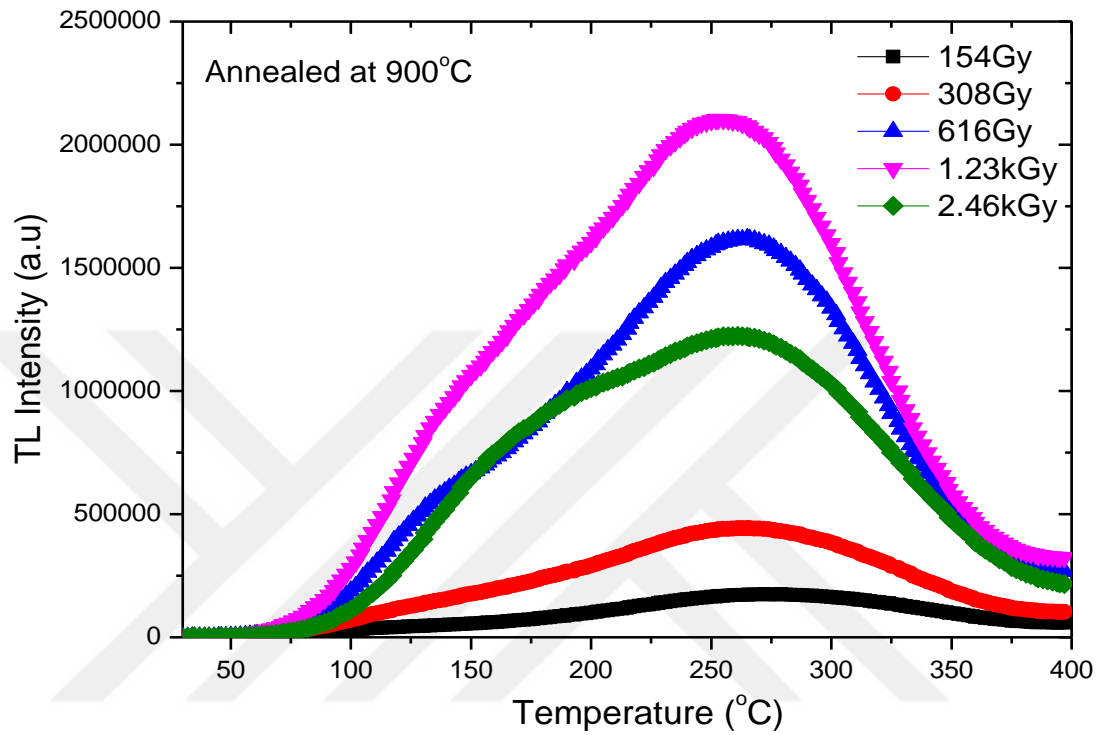


**Figure 4.6** Variation of shape of glow curves of the sample annealed at 900 °C as a function of applied dose

#### 4.1.7 The Glow Curve Variation of Sample Annealed at 1000 °C

In Figure 4.7, variation of shape of glow curves of the sample annealed at 1000 °C as a function of applied dose were examined. The shape of glow curves do not change by using different doses.

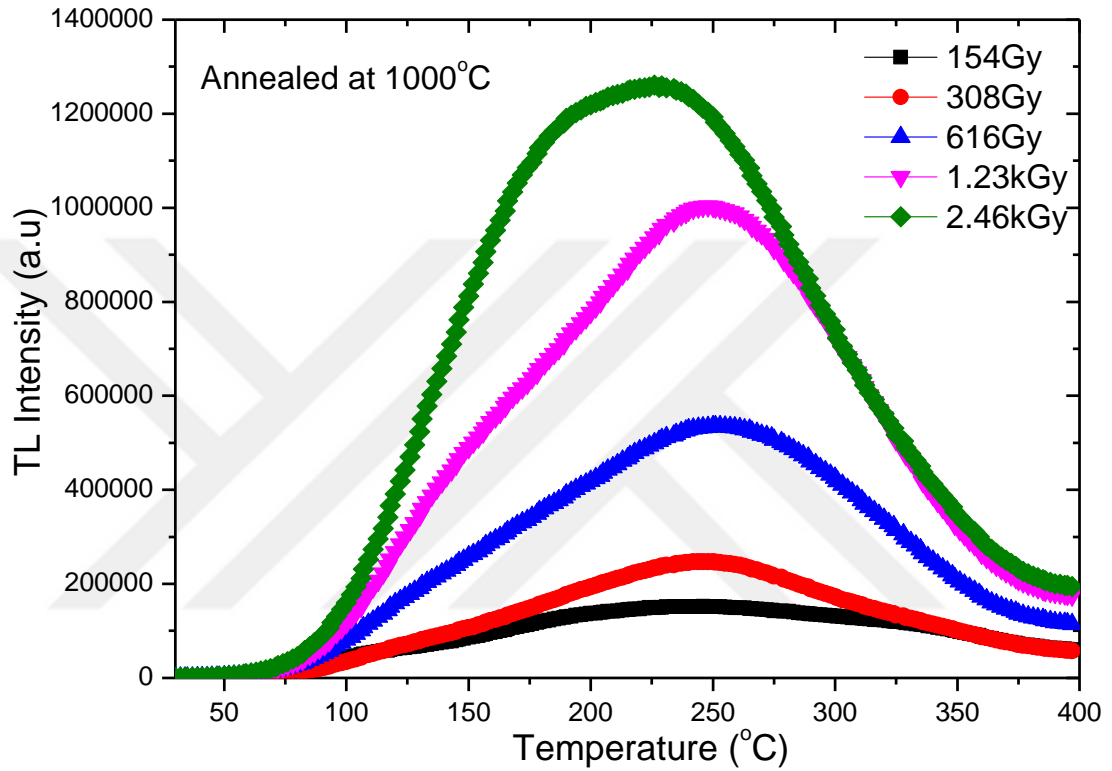


**Figure 4.7** Variation of shape of glow curves of the sample annealed at 1000 °C as a function of applied dose



#### 4.1.8 The Glow Curve Variation of Sample Annealed at 1100 °C

In Figure 4.8, variation of shape of glow curves of the sample annealed at 1100 °C as a function of applied dose were examined. The shape of glow curves do not change by using different doses. But, in the low dose region from 154 Gy to 308 Gy, the shape of glow curve changes and two separated peaks which located around 200 and 350 °C are seen. At these doses, the structure of traps and the number of traps are being changed.

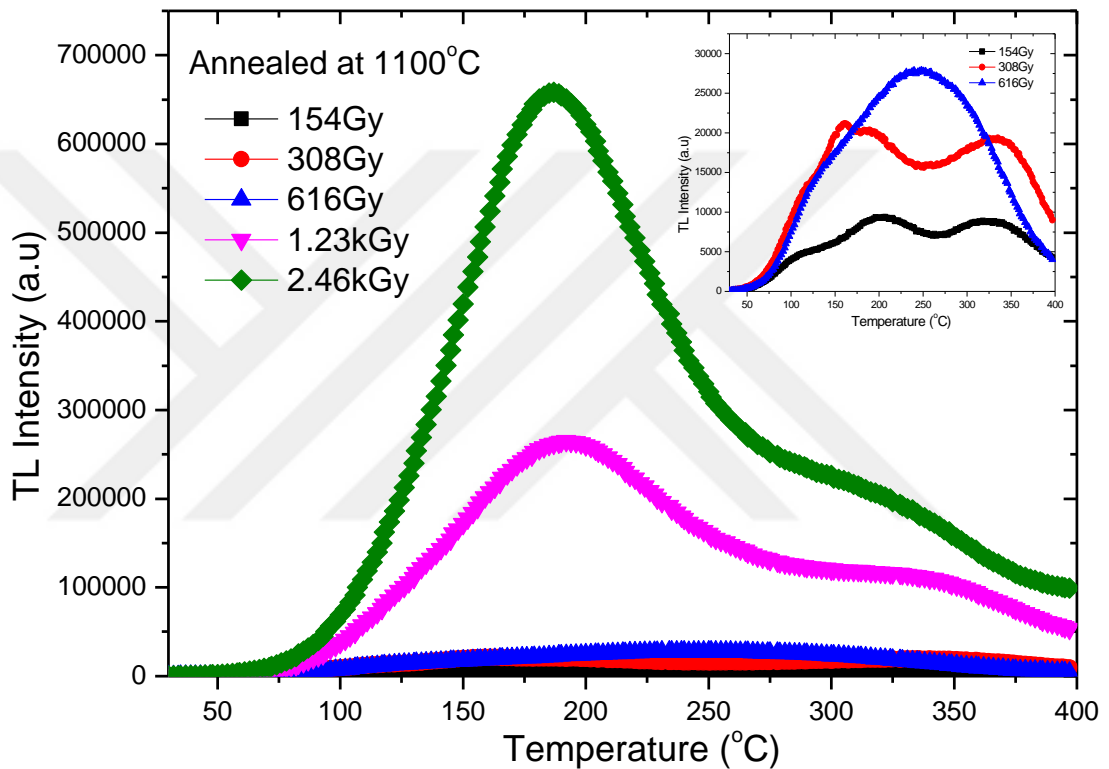


**Figure 4.8** Variations of shape of glow curves of the sample annealed at 1100 °C as a function of applied dose

Generally, the glow curve does not change by different dose values. But, annealing at different temperatures may change the glow curve shape.

## 4.2 Variation of TL Peak Intensity

In this part of the study, the effects of the different doses on the thermoluminescence peak intensity were examined.

### 4.2.1 Variation of TL Peak Intensity of Sample at 400 °C

Figure 4.9 shows the variation of the thermoluminescence peak intensity as a function of doses for the tooth enamel at 400 °C. In the low dose region, from 154 Gy to 616 Gy, the graph nearly acts as a sublinear. After 616 Gy dose value, graph becomes linear.

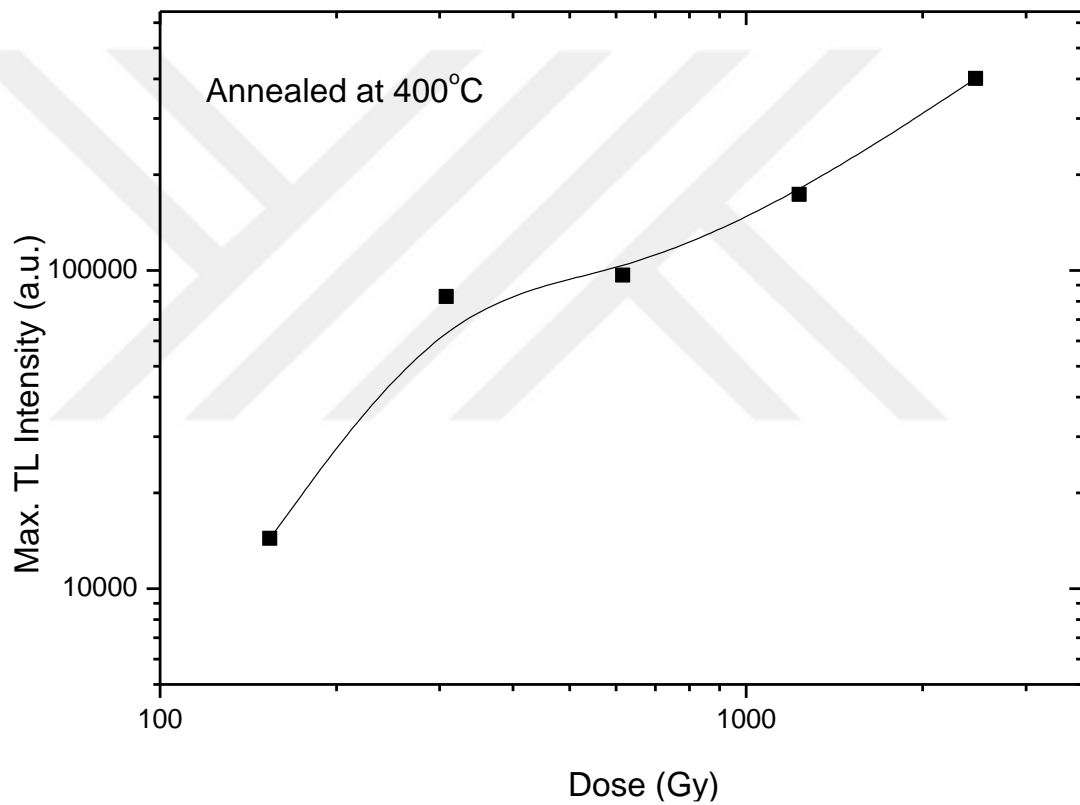


**Figure 4.9** The TL peak intensity variation of the sample annealed at 400 °C as a function of applied dose

#### 4.2.2 Variation of The TL Peak Intensity of Sample at 500 °C

Figure 4.10 shows the variation of the thermoluminescence peak intensity as a function of doses for the tooth enamel at 500 °C. In the low dose region, from 154 Gy to 308 Gy, the graph nearly acts as a sublinear. From 308 Gy to 1.23 kGy, the graph line becomes linear. After 1.23 kGy dose, graph becomes sublinear.

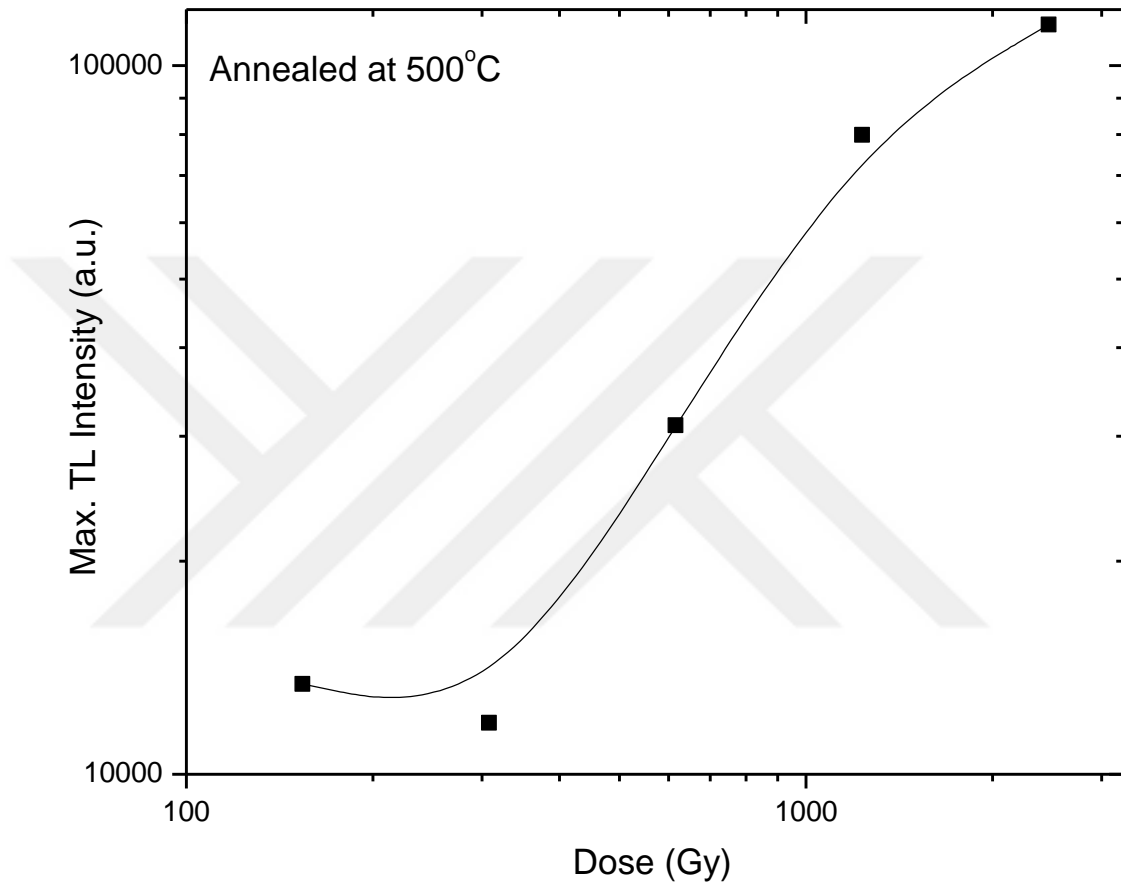


**Figure 4.10** The maximum TL intensity variations of the sample annealed at 500 °C as a function of applied dose

### 4.2.3 Variation of The TL Peak Intensity of Sample at 600 °C

Figure 4.11 shows the variation of the thermoluminescence peak intensity as a function of doses for the tooth enamel at 600 °C. In the low dose region, from 154 Gy to 308 Gy, the graph nearly acts as a sublinear. From 308 Gy to 616 Gy, the graph line becomes supralinear. After 616 Gy dose, graph becomes linear.

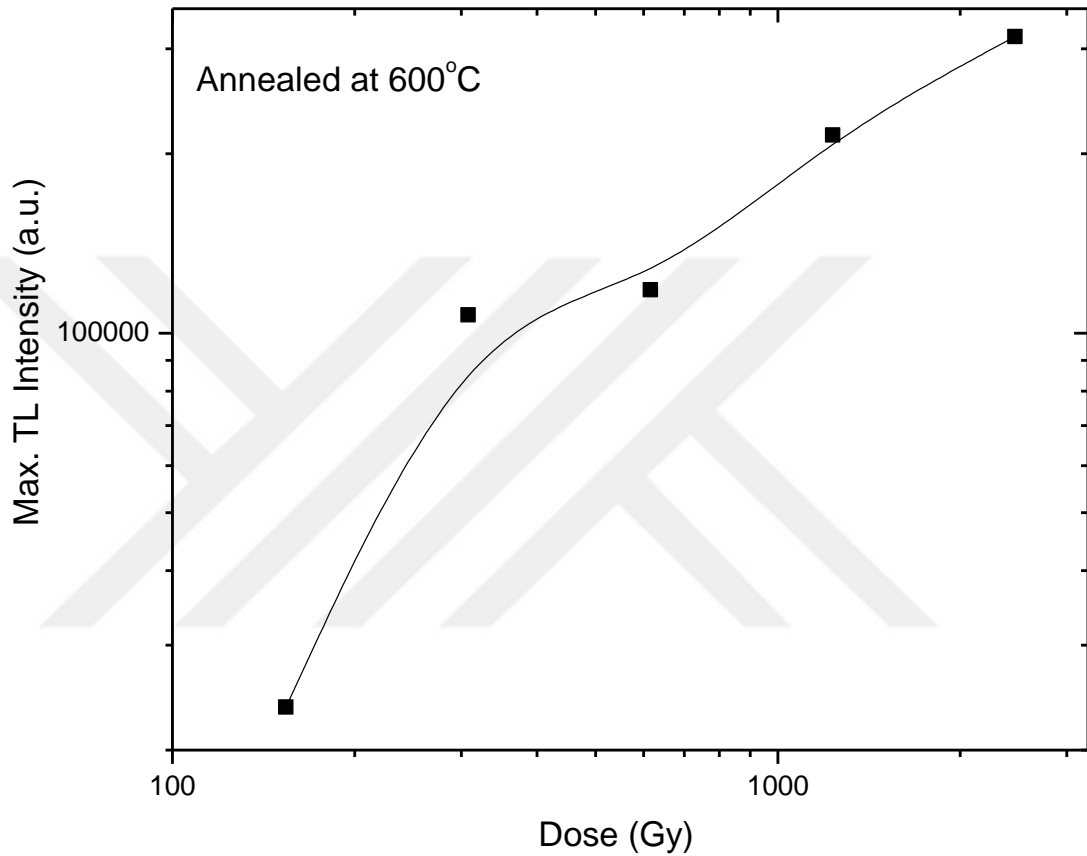


**Figure 4.11** The TL peak intensity variations of the sample annealed at 600 °C as a function of applied dose

#### 4.2.4 Variations of The TL Peak Intensity of Sample at 700 °C

Figure 4.12 shows the variations of the maximum thermoluminescence intensity as a function of doses for the tooth enamel at 700 °C. In the low dose region, from 154 Gy to 616 Gy, the graph nearly acts as a linear. After 616 Gy dose, graph becomes sublinear.

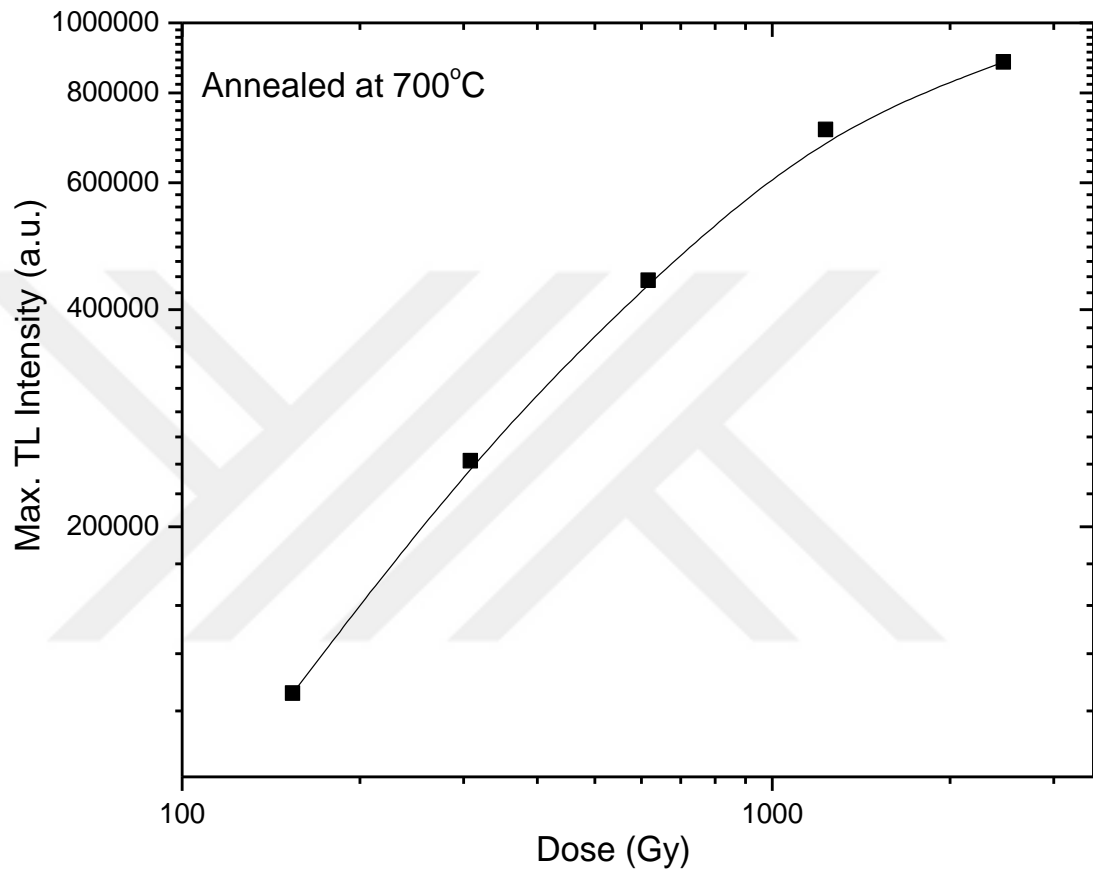


**Figure 4.12** The TL peak intensity variations of the sample annealed at 700 °C as a function of applied dose

#### 4.2.5 Variations of The TL Peak Intensity of Sample at 800 °C

Figure 4.13 shows the variations of the maximum thermoluminescence intensity as a function of doses for the tooth enamel at 800 °C. In the low dose region, from 154 Gy to 308 Gy, the graph nearly acts as a supralinear. From 308 Gy to 616 Gy, the graph line becomes linear. After 616 Gy dose, graph becomes sublinear.

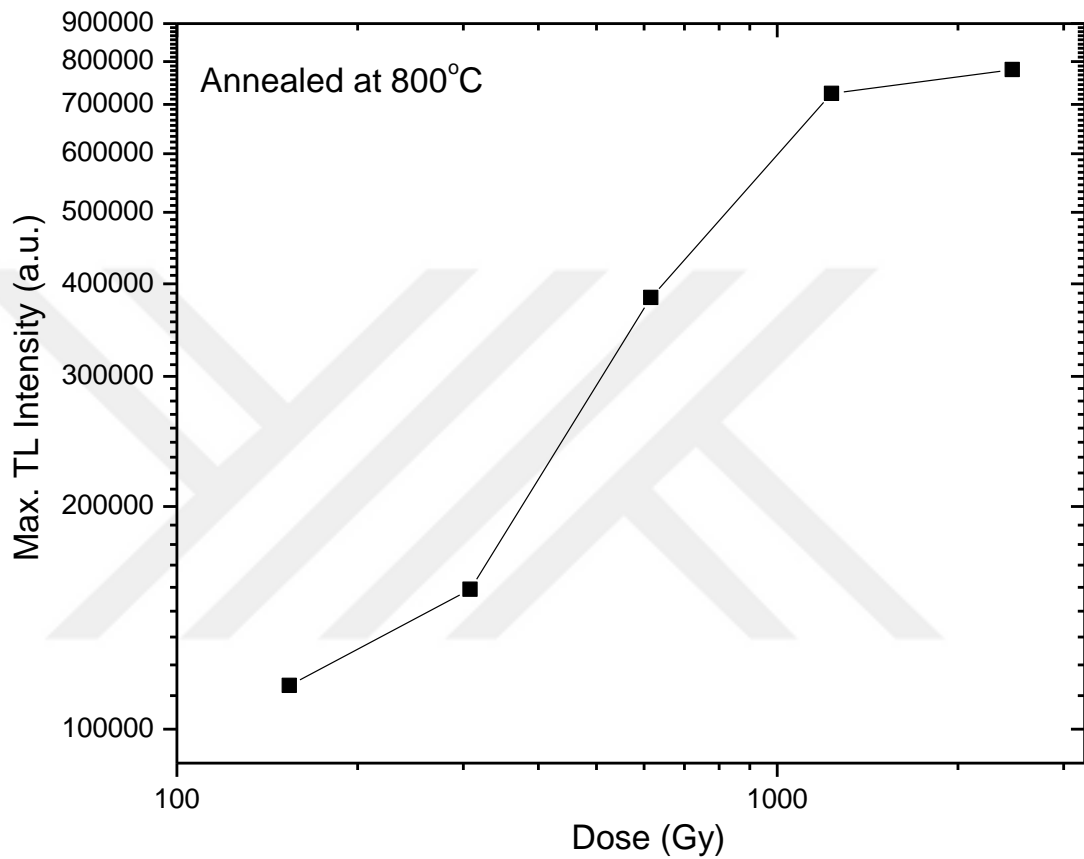


**Figure 4.13** The TL peak intensity variations of the sample annealed at 800 °C as a function of applied dose

#### 4.2.6 Variations of The TL Peak Intensity of Sample at 900 °C

Figure 4.14 shows the variations of the maximum thermoluminescence intensity as a function of doses for the tooth enamel at 900 °C. In the low dose region, from 154 Gy to 616 Gy, the graph nearly acts as a linear. After 616 Gy dose, graph becomes sublinear.

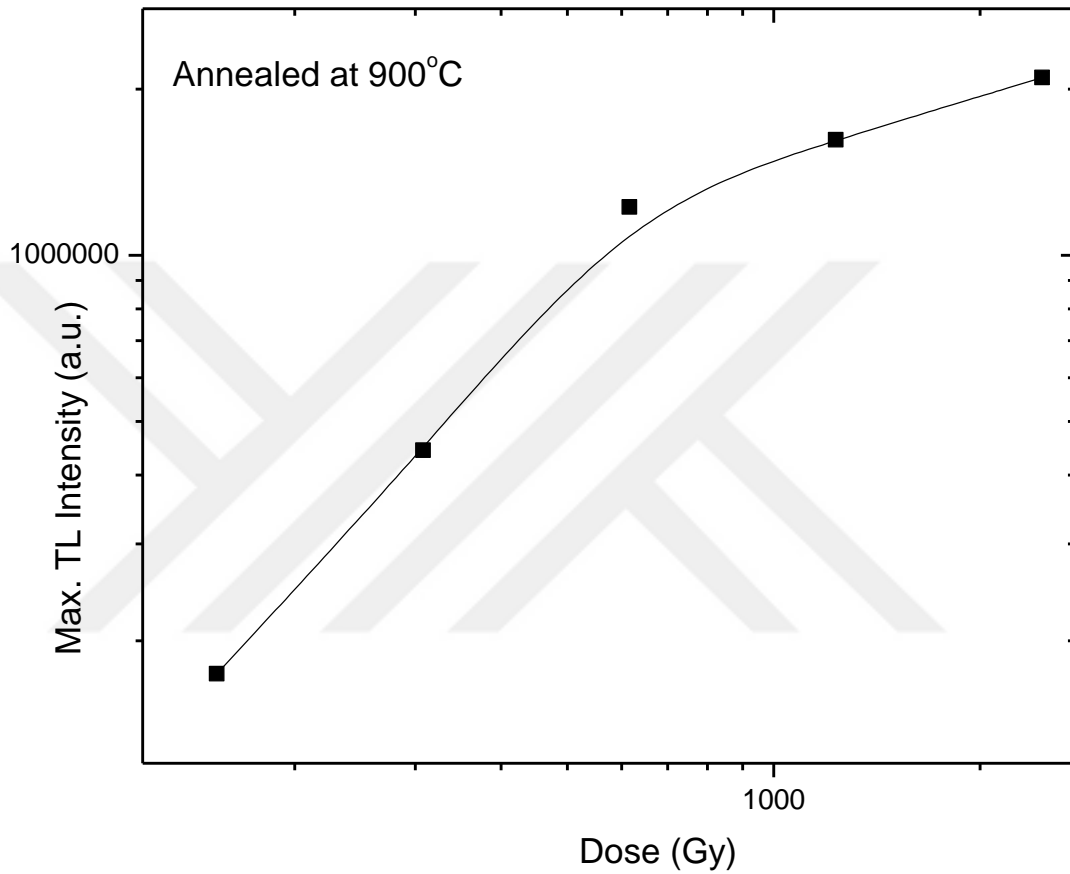


**Figure 4.14** The TL peak intensity variations of the sample annealed at 900 °C as a function of applied dose

#### 4.2.7 Variations of The TL Peak Intensity of Sample at 1000 °C

Figure 4.15 shows the variations of the maximum thermoluminescence intensity as a function of doses for the tooth enamel at 1000 °C. In the low dose region, from 154 Gy to 308 Gy, the graph nearly acts as a supralinear. From 308 Gy to 1.23 kGy, the graph line becomes linear. After 1.23 kGy dose, graph becomes sublinear.

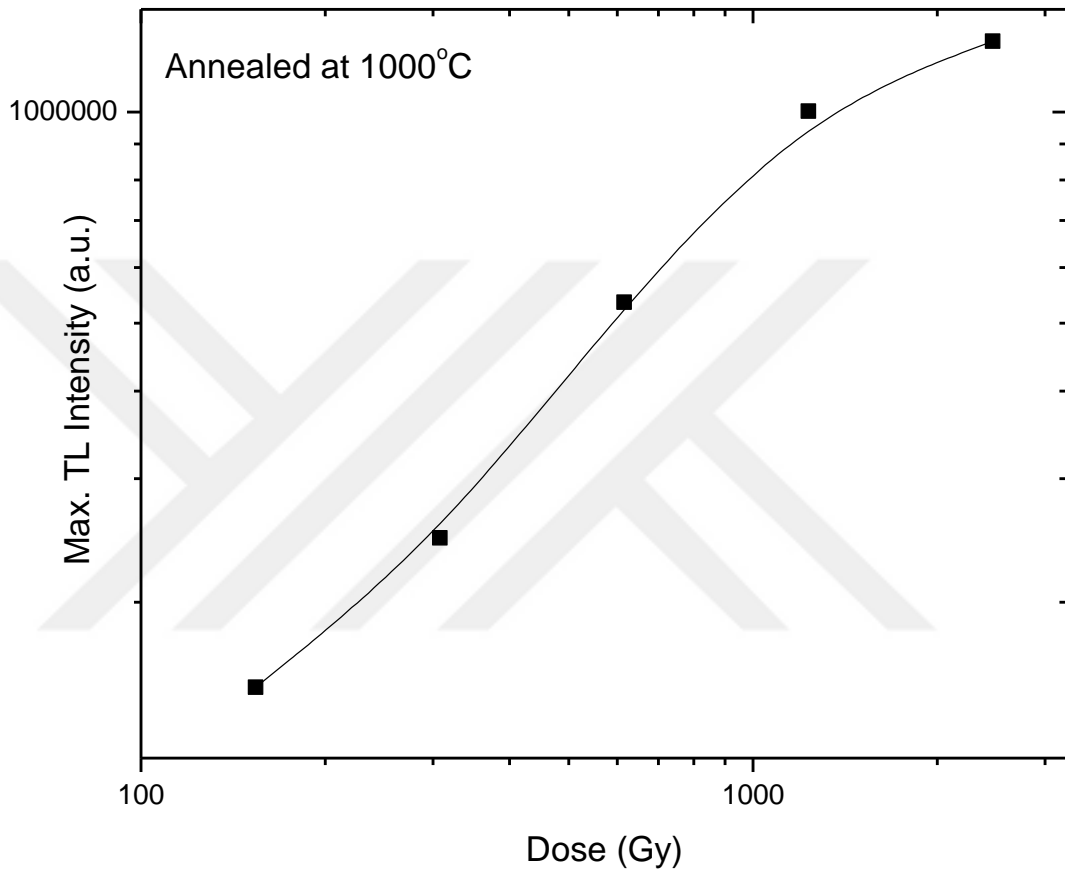


**Figure 4.15** The TL peak intensity variations of the sample annealed at 1000 °C as a function of applied dose



#### 4.2.8 Variations of The TL Peak Intensity of Sample at 1100 °C

Figure 4.16 shows the variations of the maximum thermoluminescence intensity as a function of doses for the tooth enamel at 1100 °C. In the low dose region, from 154 Gy to 308 Gy, the graph nearly acts as a linear. From 308 Gy to 616 Gy, the graph line becomes sublinear. After 616 Gy dose, graph becomes supralinear.

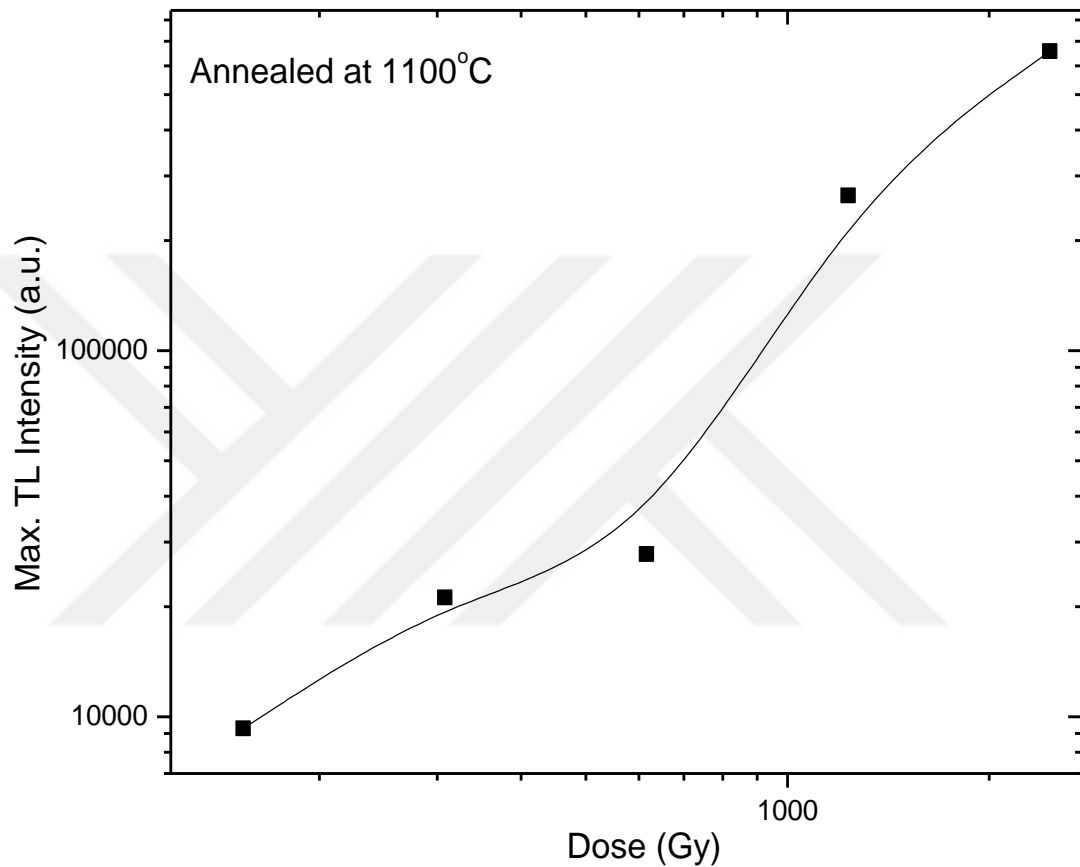


**Figure 4.16** The TL peak intensity variations of the sample annealed at 1100 °C as a function of applied dose

### 4.3 The Area Under The Curve:

In this part of the experiment, the effects of the different doses on the peak area were investigated.

#### 4.3.1 The Area Under The Curve Variations of Sample at 400 °C

Figure 4.17 shows the variation of area under curve as a function of dose for the tooth enamel at 400 °C. In Figure 4.17, in the low dose region, from 154 Gy to 308 Gy, peak area increases with increasing dose and acts as a supralinear. From 308 Gy to 616 Gy, the graph line becomes linear and peak area increases with increasing dose. For the other dose regions, from 616 Gy to 2.46 Gy, the graph line becomes sublinear. The expectation for dose versus peak area graph is linearly increase. And the graph generally increases linearly. This graph is drawn also on logarithmic scale.

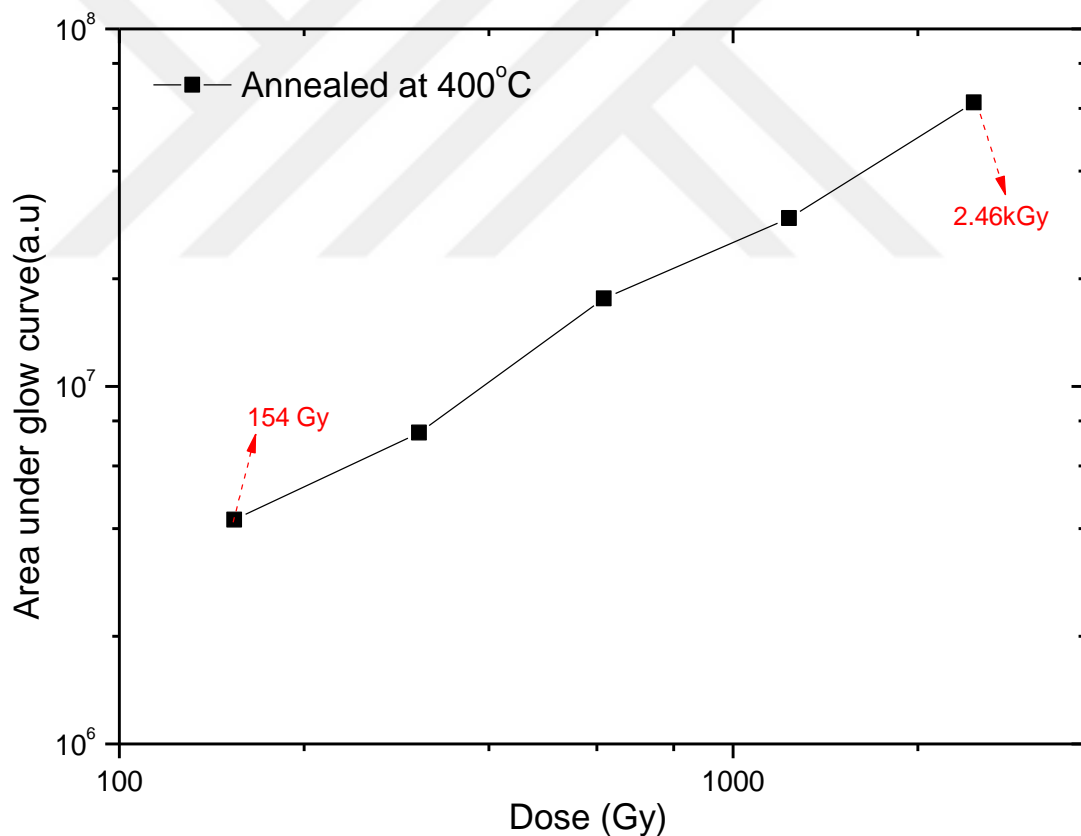


**Figure 4.17** The area under the curve variations of the sample annealed at 400 °C as a function of applied dose

### 4.3.2 The Area Under The Curve Variations of Sample at 500 °C

Figure 4.18 shows the variation of area under curve as a function of dose for the tooth enamel at 500 °C. In Figure 4.18, in the low dose region, from 154 Gy to 308 Gy, peak area increases with increasing dose and acts as a supralinear. From 308 Gy to 1.23 Gy, the graph line becomes linear and peak area increases with increasing dose. For the high dose region, 2.46 Gy dose, the graph line becomes sublinear. The expectation for dose versus peak area graph is linearly increase. And the graph generally increases linearly. This graph is drawn also on logarithmic scale.

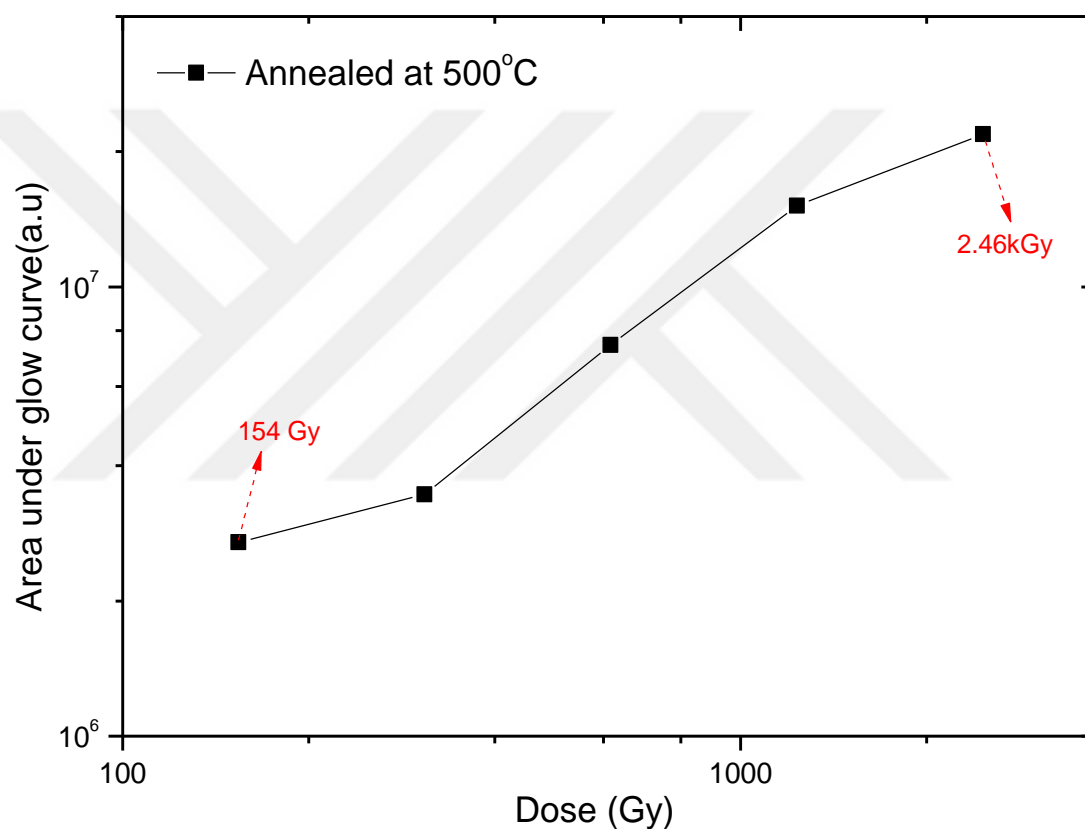


**Figure 4.18** The area under the curve variations of the sample annealed at 500 °C as a function of applied dose

### 4.3.3 The Area Under The Curve Variations of Sample at 600 °C

Figure 4.19 shows the variation of area under curve as a function of dose for the tooth enamel at 600 °C. In Figure 4.18, firstly between at 154 Gy 616 Gy, the graph line increases slowly with increasing dose and acts as sublinear. From 616 Gy to 2.46 kGy, the graph line becomes nearly linear and peak area linearly increases with increasing dose. This graph is drawn also on logarithmic scale.

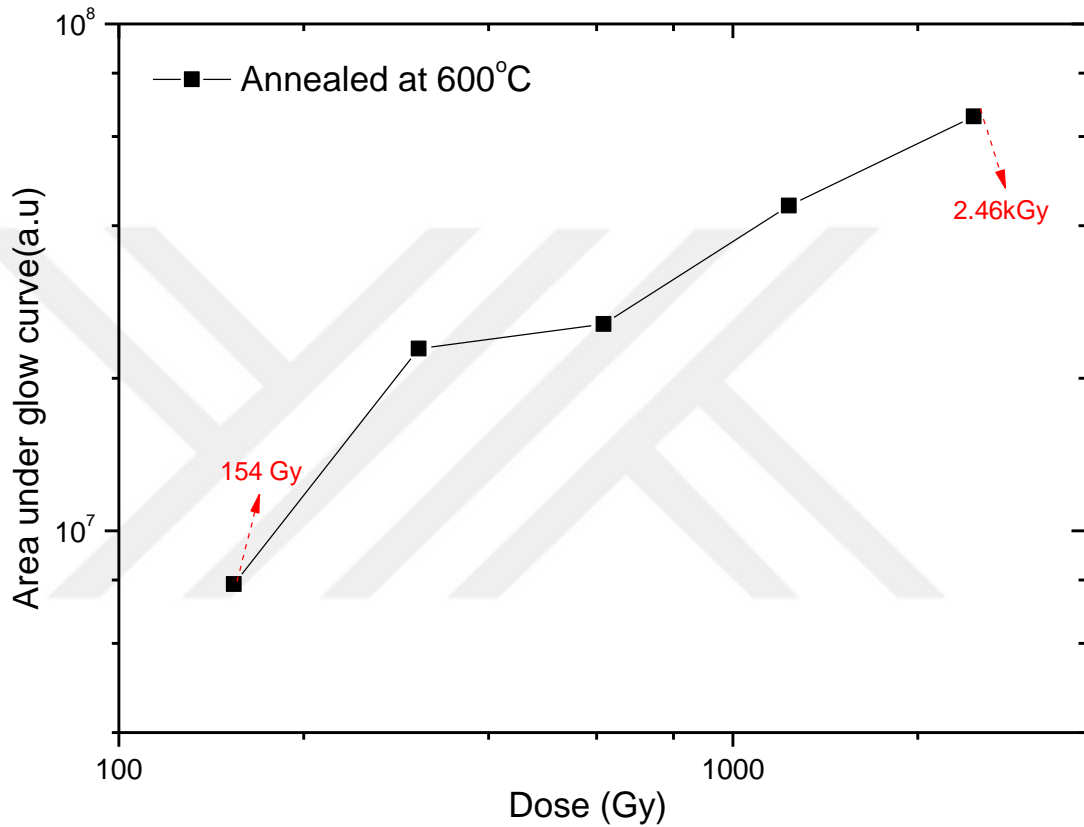


**Figure 4.19** The area under the curve variations of the sample annealed at 600 °C as a function of applied dose

#### 4.3.4 The Area Under The Curve Variations of Sample at 700 °C

Figure 4.20 shows the variation of area under curve as a function of doses for the tooth enamel at 700 °C. In Figure 4.20, in the dose regions from 154 Gy to 1.23 kGy, peak area increases with increasing dose and acts as a linear. After, in the high dose region 2.46 kGy dose, graph becomes sublinear. The expectation for dose versus peak area graph is linearly increase. This graph is drawn also on logarithmic scale.

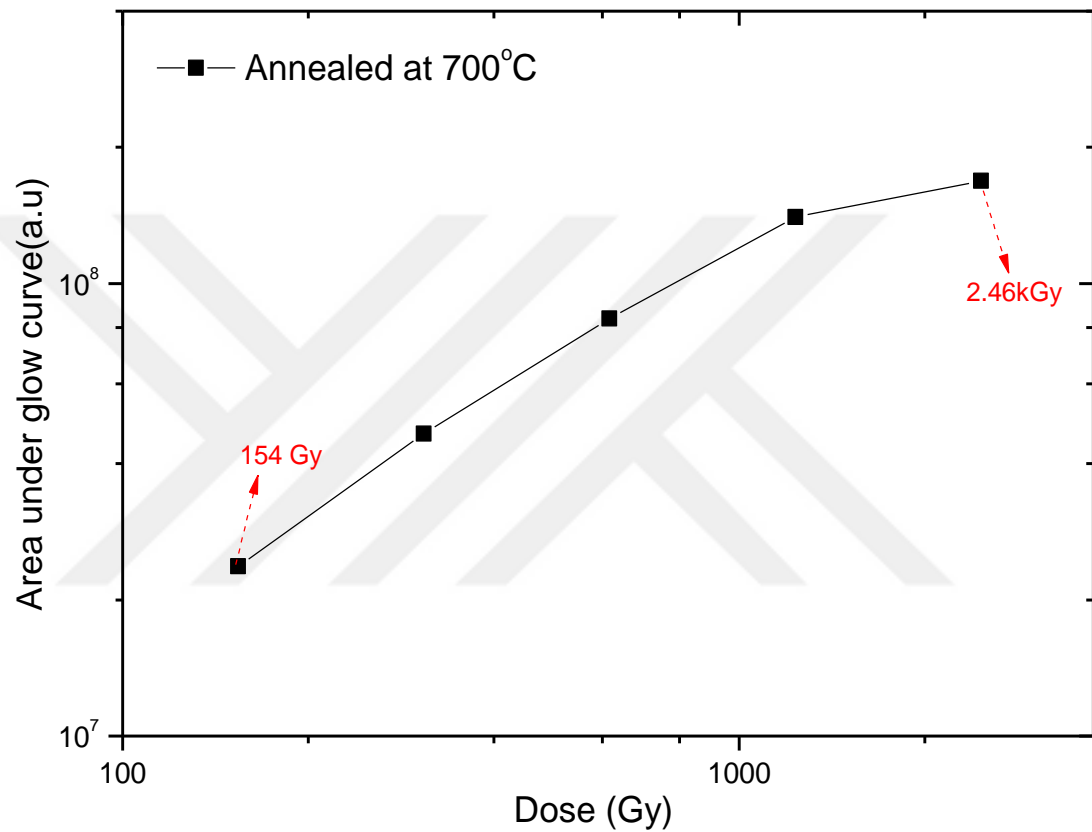


**Figure 4.20** The area under the curve variations of the sample annealed at 700 °C as a function of applied dose

### 4.3.5 The Area Under The Curve Variations of Sample at 800 °C

Figure 4.21 shows the variation of area under curve as a function of doses for the tooth enamel at 800 °C. In Figure 4.21, in the dose region, from 154 Gy to 616 Gy, the graph line increases quickly with increasing dose and acts as a supralinear. From 616 Gy to 2.46 kGy, the graph line becomes sublinear and peak area slowly increases with increasing dose. This graph is drawn also on logarithmic scale.

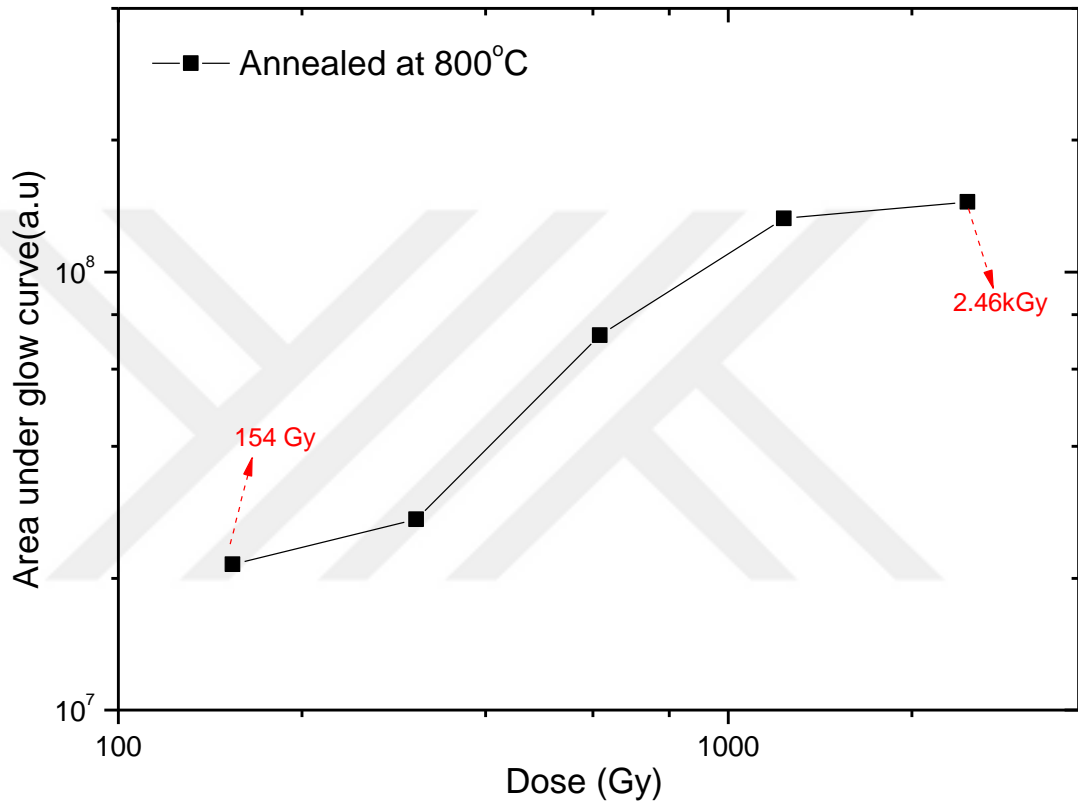


**Figure 4.21** The area under the curve variations of the sample annealed at 800 °C as a function of applied dose

#### 4.3.6 The Area Under The Curve Variations of Sample at 900 °C

Figure 4.22 shows the variations of the maximum thermoluminescence intensity as a function of dose for the tooth enamel at 900 °C. In the low dose region, from 154 Gy to 616 Gy, the graph nearly acts as a linear. From 616 Gy to 2.46 kGy, the area under the curve reaches to its saturation value and the graph becomes sublinear. This graph is drawn also on logarithmic scale.

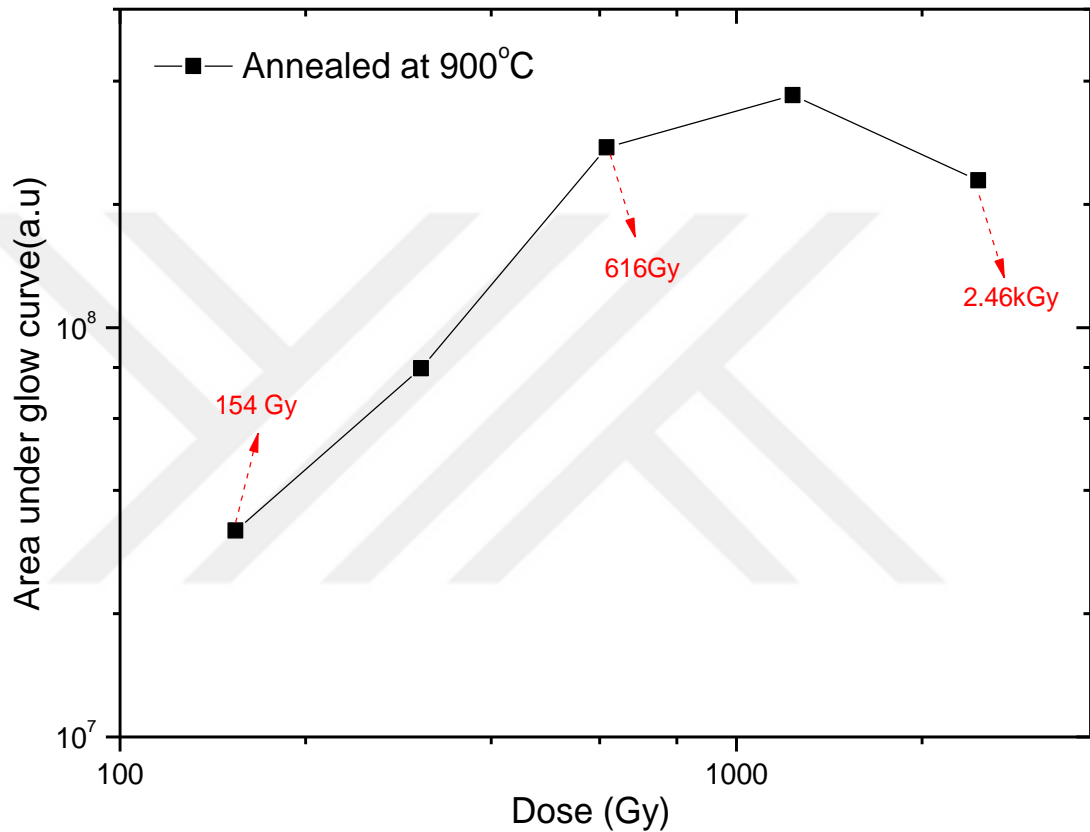


**Figure 4.22** The area under the curve variations of the sample annealed at 900 °C as a function of applied dose

### 4.3.7 The Area Under The Curve Variations of Sample at 1000 °C

Figure 4.23 shows the variation of area under curve as a function of dose for the tooth enamel at 1000 °C. In Figure 4.23, in the low dose region, from 154 Gy to 616 Gy, the graph line increases quickly with increasing dose and acts as a supralinear. From 616 Gy to 2.46 kGy, peak area slowly increases with increasing dose and the graph line becomes sublinear.

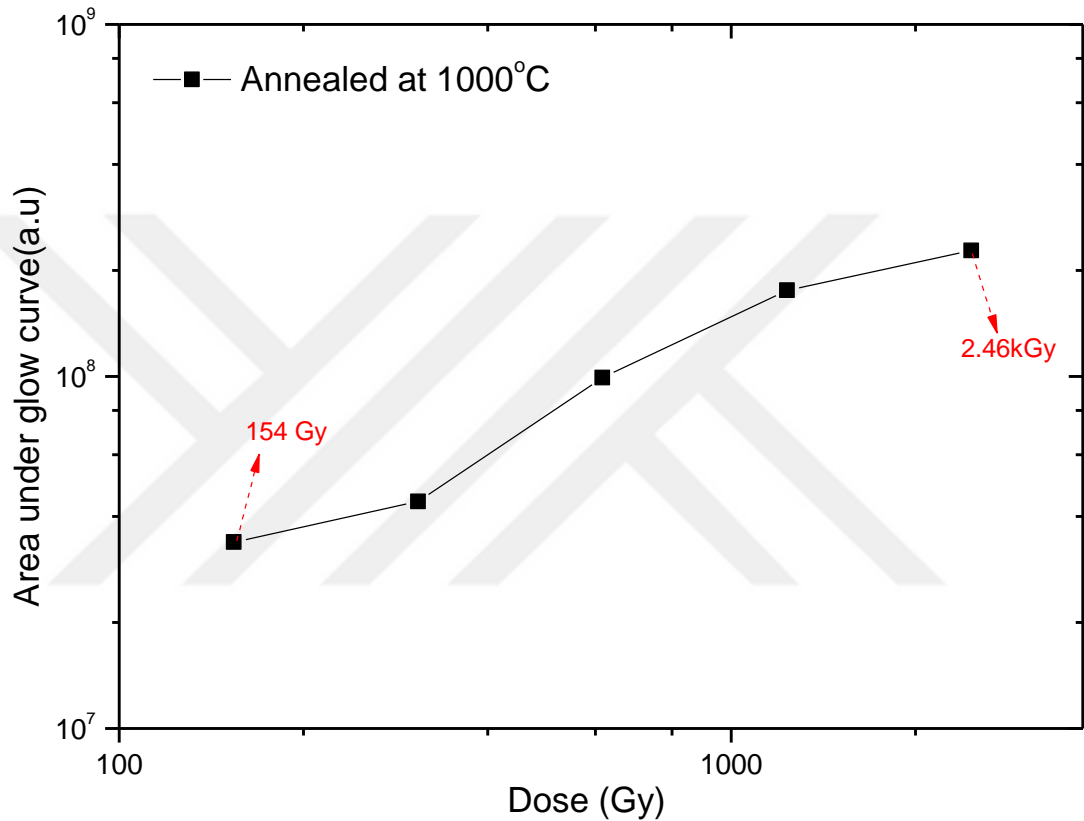


**Figure 4.23** The area under the curve variations of the sample annealed at 1000 °C as a function of applied dose



### 4.3.8 The Area Under The Curve Variations of Sample at 1100 °C

Figure 4.24 shows the variation of area under curve as a function of doses for the tooth enamel at 1100 °C. In Figure 4.24, between 154 Gy to 2.46 kGy, the dose response acts as a linear. We think that there is an experimental error at 616 Gy. This graph is drawn also on logarithmic scale.

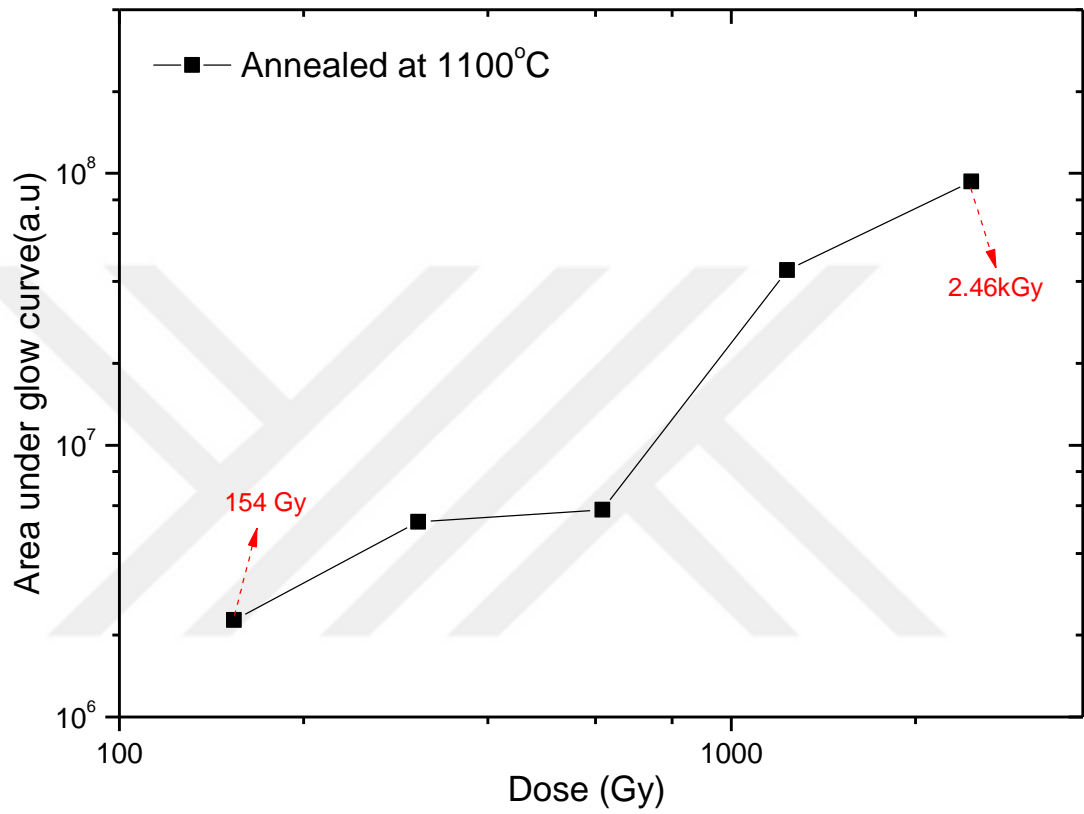


**Figure 4.24** The area under the curve variations of the sample annealed at 1100 °C as a function of applied dose

#### 4.4 Peak Temperature

In this part of the experiment, the effects of the different doses on the TL peak temperature were investigated.

##### 4.4.1 Variations of TL Peak Temperature of Sample at 400 °C

Figure 4.25 shows the variation of TL peak temperature as a function of doses for the tooth enamel annealed at 400 °C. In Figure 4.25, the TL peak temperature shifts to higher temperature region with increasing applied dose. This shifting is about 20 °C until 1.23 kGy. After 1.23 kGy, the TL peak temperature decreases about 10 °C. Generally, the TL peak temperature of the sample annealed at 400 °C shifts to higher temperature region about 20 °C between 154 Gy and 2.46 kGy.

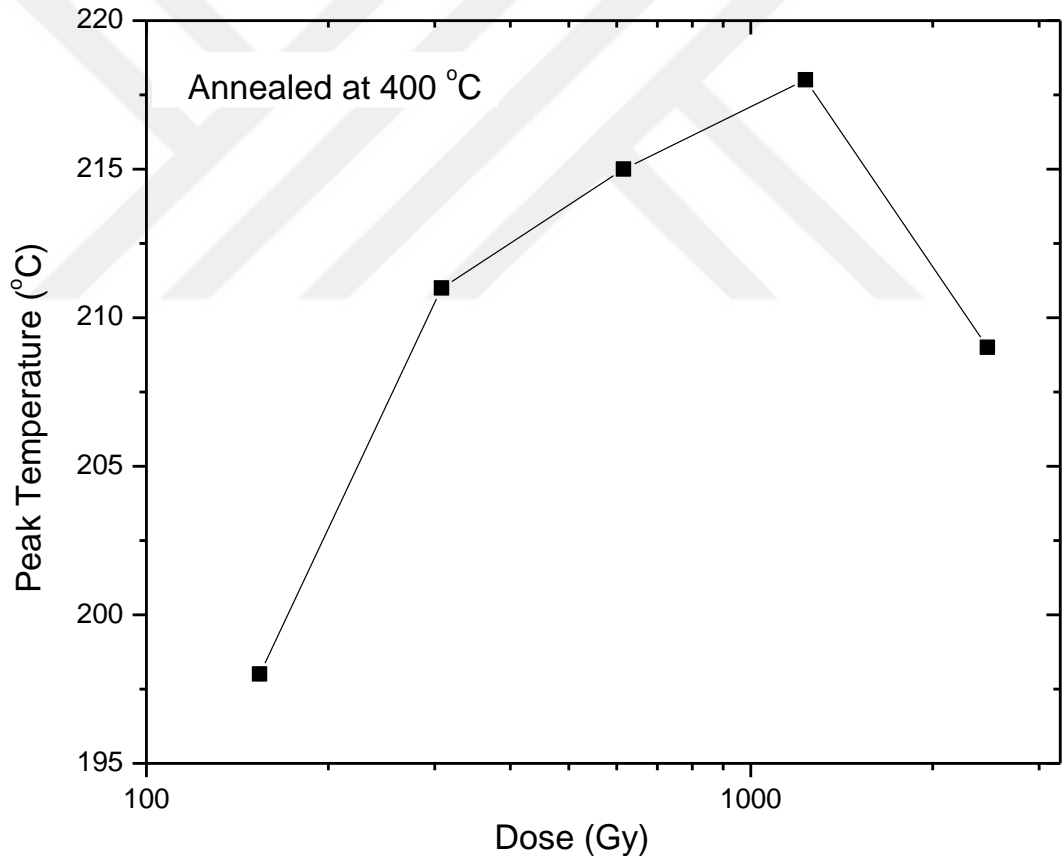


**Figure 4.25** The peak temperature variations of the sample annealed at 400 °C as a function of applied dose

#### 4.4.2 Variations of TL Peak Temperature of Sample at 500 °C

Figure 4.26 shows the variation of TL peak temperature as a function of doses for the tooth enamel at 500 °C. In that figure, the TL peak temperature shifts to lower temperature region with increasing applied dose until 616 Gy. This shifting is about nearly 3 °C. Between 616 Gy and 1.23 kGy, the TL peak temperature increases 6 °C. After 1.23 kGy, the TL peak temperature decreases 6 °C. Generally, there is no important change in the TL peak temperature of the sample annealed at 500 °C

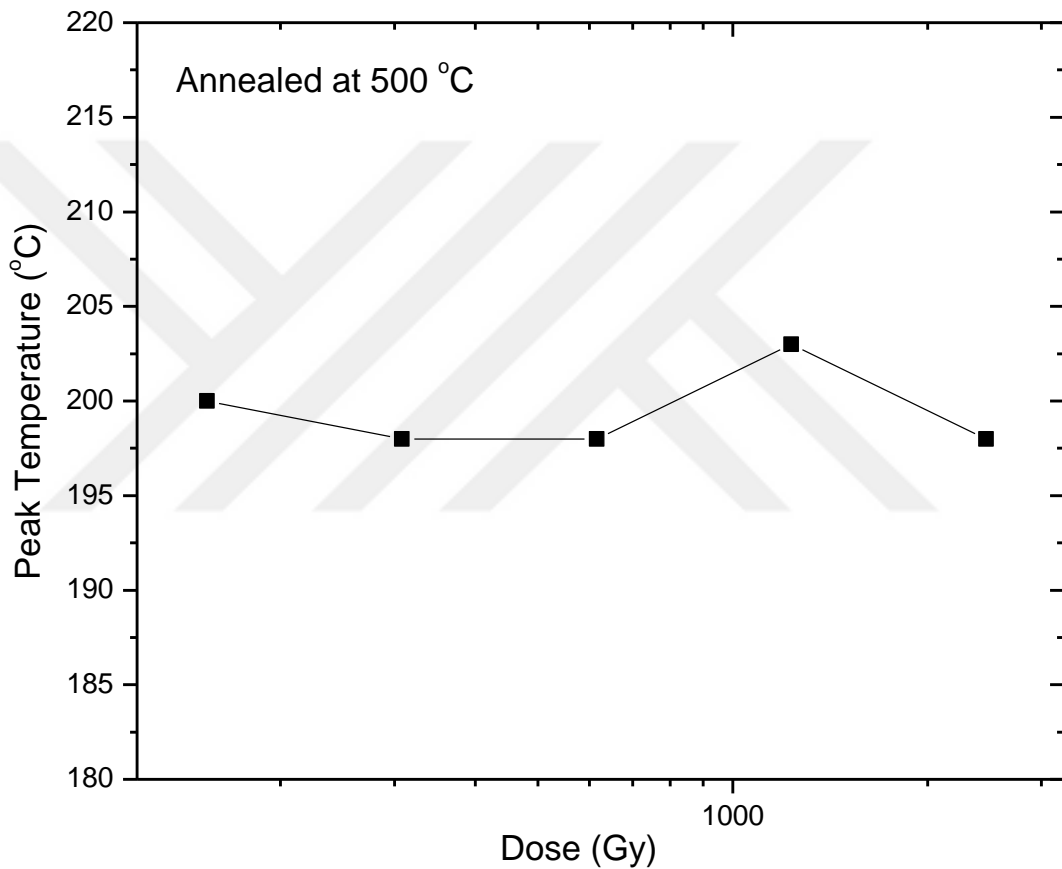


**Figure 4.26** The TL peak temperature variations of the sample annealed at 500 °C as a function of applied dose

#### 4.4.3 Variations of TL Peak Temperature of Sample at 600 °C

Figure 4.27 shows the variation of TL peak temperature as a function of dose for the tooth enamel annealed at 600 °C. In Figure 4.27, the TL peak temperature increases nearly 40 °C until 308 Gy. Then, between 308 Gy and 616 Gy, the TL peak temperature decreases about 40 °C. After that, the TL peak temperature increases nearly 15 °C up to 2.46 kGy. Generally, the TL peak temperature of the sample annealed at 600 °C shifts to higher temperature region about 15 °C between 154 Gy and 2.46 kGy.

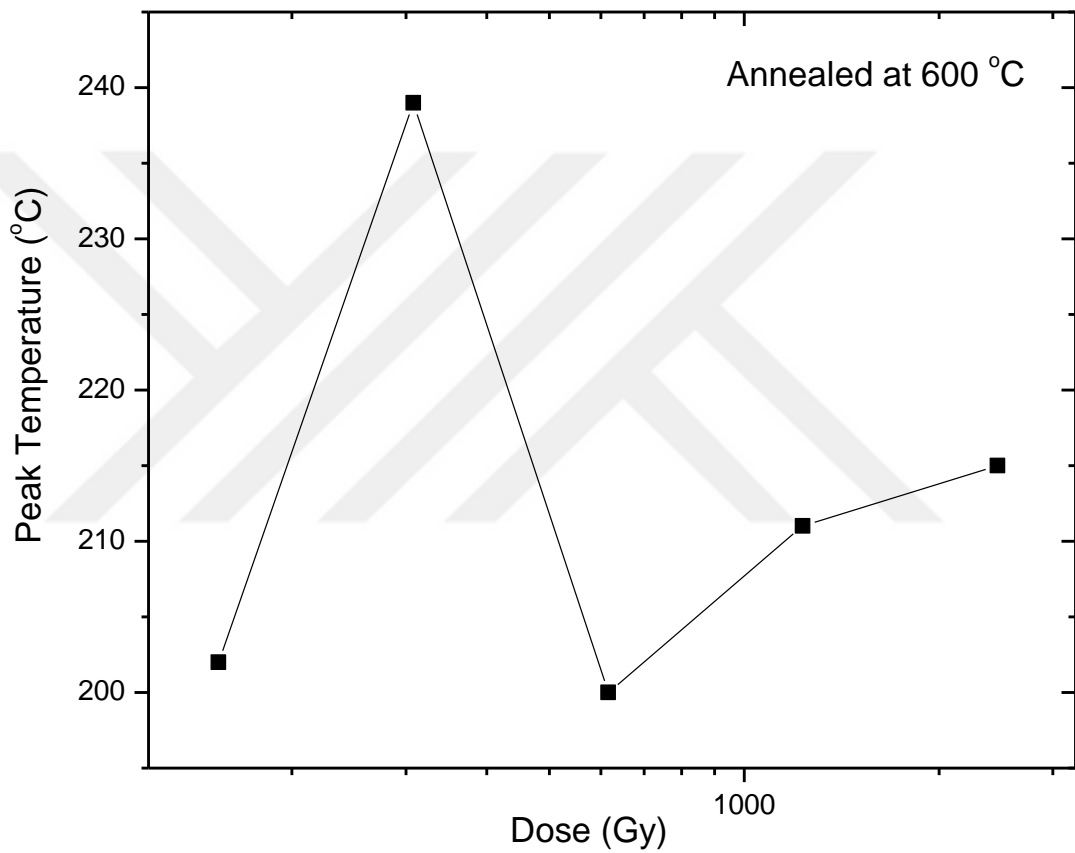


**Figure 4.27** The TL peak temperature variations of the sample annealed at 600 °C as a function of applied dose

#### 4.4.4 Variations of TL Peak Temperature of Sample at 700 °C

Figure 4.28 shows the variation of TL peak temperature as a function of dose for the tooth enamel annealed at 700 °C. In that figure, the TL peak temperature does not change until 308 Gy. Then, between 308 Gy and 2.46 kGy, the TL peak temperature decreases nearly 23 °C. Generally, the TL peak temperature of the sample annealed at 700 °C shifts to lower temperature region about 25 °C between 154 Gy and 2.46 kGy.

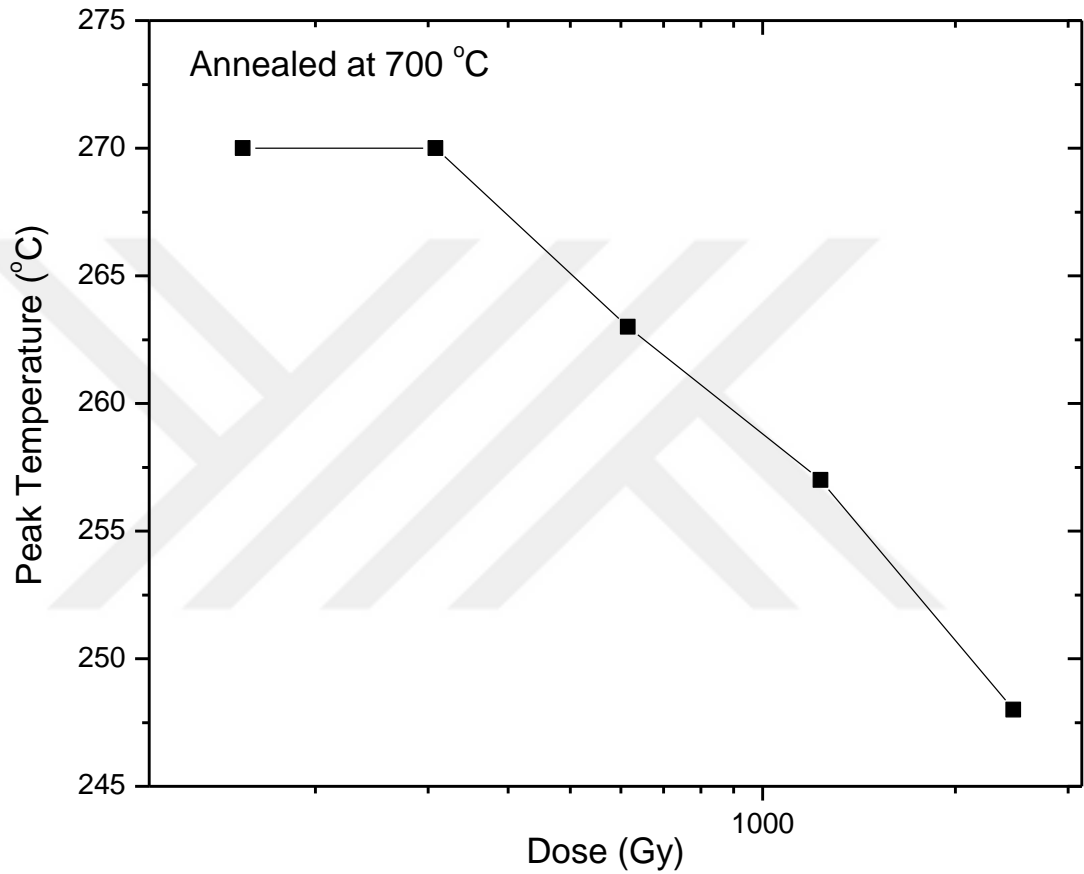


**Figure 4.28** The TL peak temperature variations of the sample annealed at 700 °C as a function of applied dose

#### 4.4.5 Variations of TL Peak Temperature of Sample at 800 °C

Figure 4.29 shows the variation of TL peak temperature as a function of dose for the tooth enamel annealed at 800 °C. In Figure 4.29, the TL peak temperature increases nearly 5 °C until 308 Gy. Then, between 308 Gy and 1.23 kGy, the TL peak temperature decreases about 10 °C. Also, the TL peak temperature does not change between 1.23 kGy and 2.46 kGy. Generally, there is no important change in the TL peak temperature of the sample annealed at 800 °C.

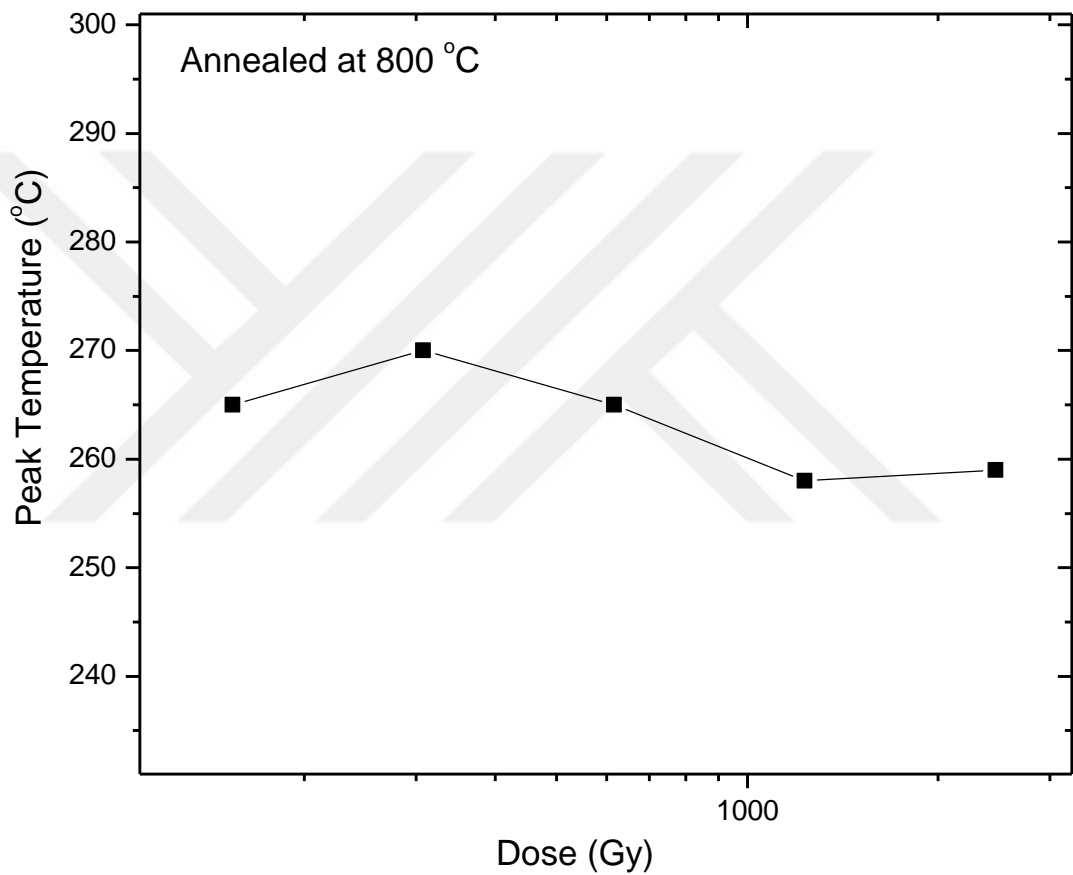


**Figure 4.29** The TL peak temperature variations of the sample annealed at 800 °C as a function of applied dose

#### 4.4.6 Variations of TL Peak Temperature of Sample at 900 °C

Figure 4.30 shows the variation of TL peak temperature as a function of dose for the tooth enamel annealed at 900 °C. In Figure 4.29, the TL peak temperature decreases nearly 20 °C until 616 Gy. Then, between 616 Gy and 1.23 kGy, the TL peak temperature increases about 5 °C. After that, the TL peak temperature decreases nearly 10 °C up to 2.46 kGy. Generally, the TL peak temperature of the sample annealed at 900 °C shifts to lower temperature region about 25 °C between 154 Gy and 2.46 kGy.

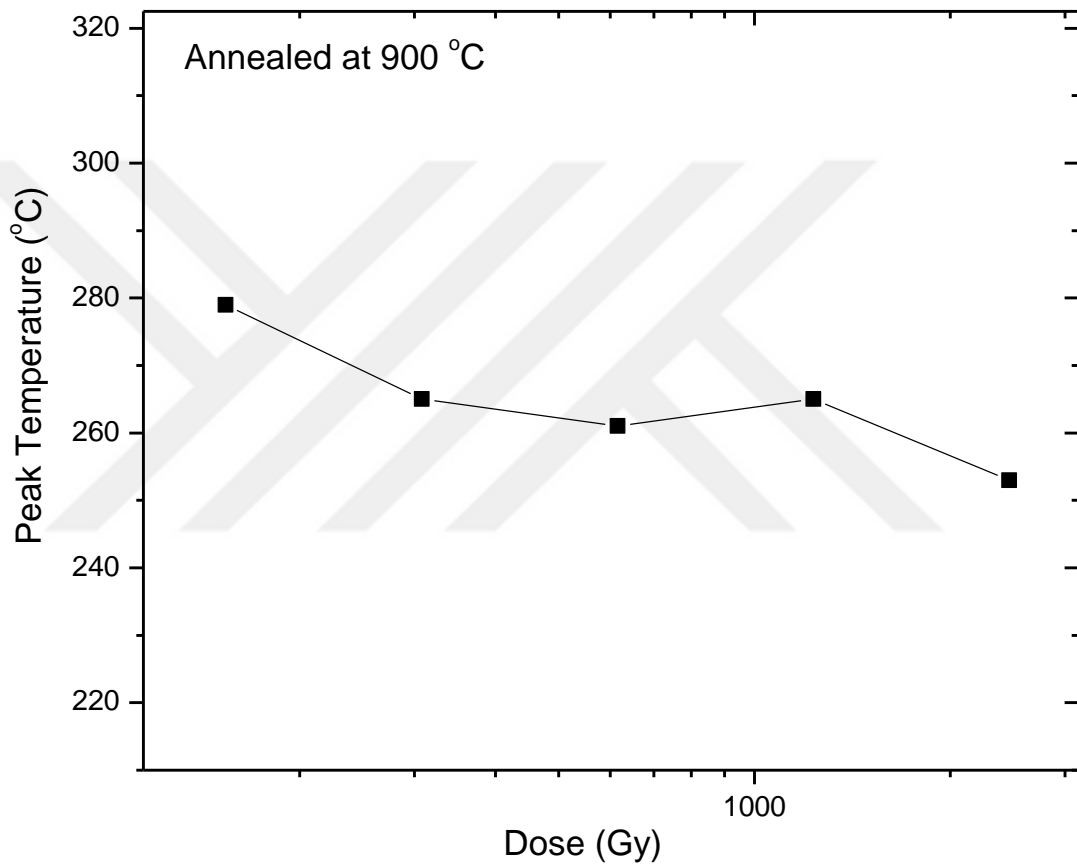


**Figure 4.30** The TL peak temperature variations of the sample annealed at 900 °C as a function of applied dose

#### 4.4.7 Variations of Peak Temperature of Sample at 1000 °C

Figure 4.31 shows the variation of TL peak temperature as a function of dose for the tooth enamel at 1000 °C. In the figure 4.31, the TL peak temperature does not change until 616 Gy. After 616 Gy, the TL peak temperature decreases nearly 25 °C. Generally, no important change is observed in the TL peak temperature of the sample annealed at 1000 °C for low dose region but a 25 °C shifting is observed for high dose region.

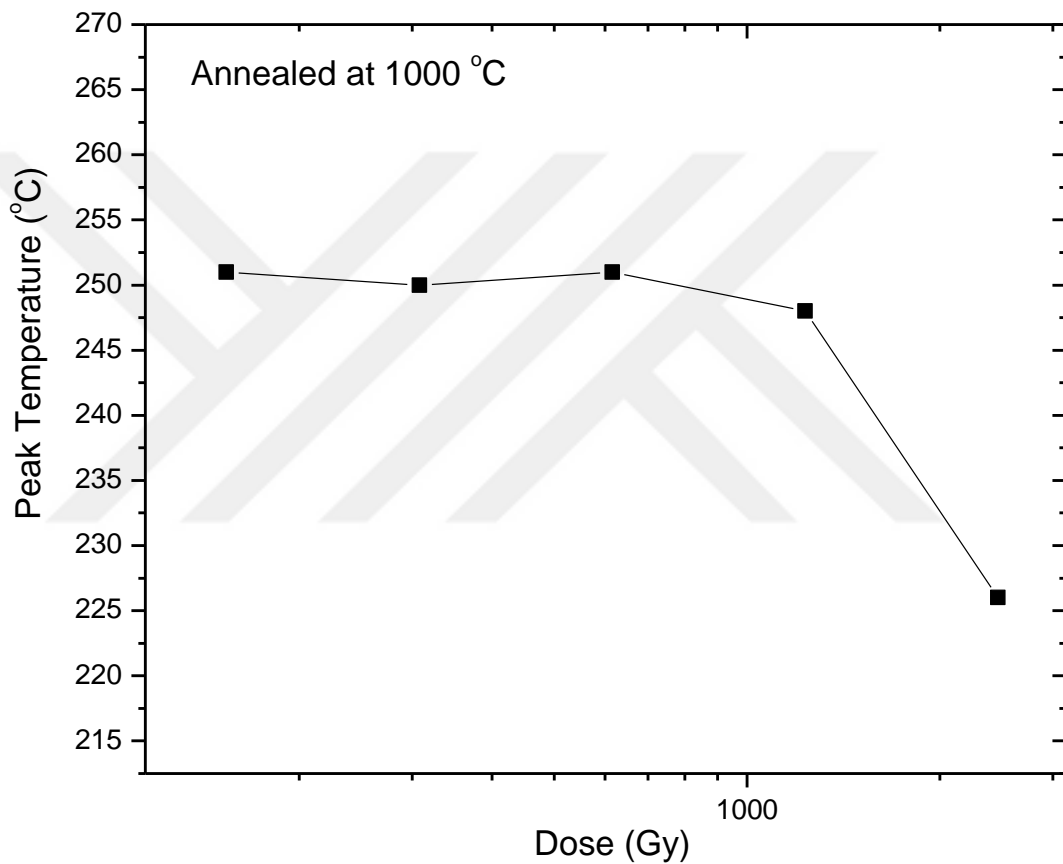


**Figure 4.31** The TL peak temperature variations of the sample annealed at 1000 °C as a function of applied dose



#### 4.4.8 Variations of TL Peak Temperature of Sample at 1100 °C

Figure 4.32 shows the variation of TL peak temperature as a function of doses for the tooth enamel at 1100 °C. In Figure 4.32, the TL peak temperature decreases about 40 °C until 308 Gy. Then, between 308 Gy and 616 Gy, the TL peak temperature increases about 80 °C. After that, the TL peak temperature decreases nearly 50 °C up to 2.46 kGy. Generally, different TL peak temperature is observed at different doses, but it is understood that the TL peak temperature of the sample annealed at 1100 °C does not affected by the dose variation.

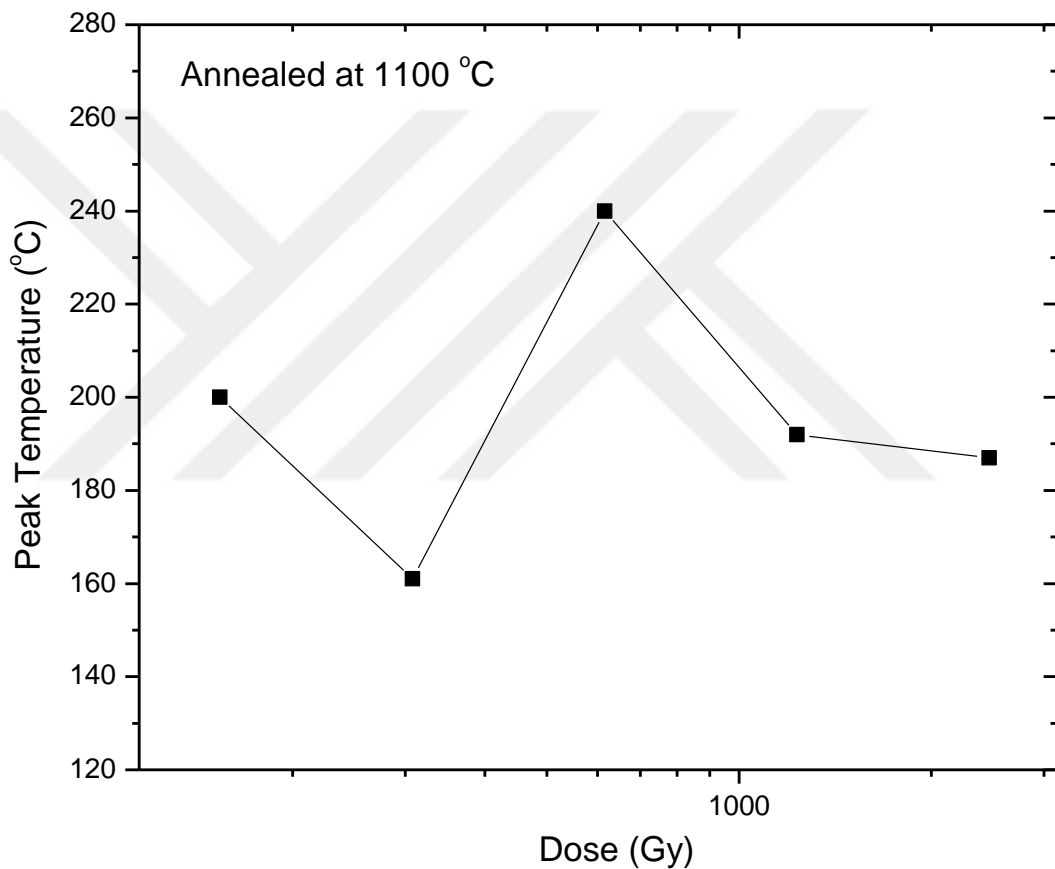


**Figure 4.32** The TL peak temperature variations of the sample annealed at 1100 °C as a function of applied dose

## CHAPTER 5

### DISCUSSION AND CONCLUSION

Human calcified tissues, such as bones and teeth, are of special interest to retrospective dosimetry. They can provide very useful information on exposure to ionizing radiation many years after the event, since the 'signal' is 'stored' in these materials. For more than three decades tooth enamel has been known as a detector for in vitro electron paramagnetic resonance (EPR) dosimetry [67]. EPR dose reconstruction by using dental enamel is based on measurements of stable radiation-induced radicals.

Thermoluminescence (TL) retrospective dosimetry using tooth enamel is potentially an interesting alternative to EPR retrospective dosimetry since it requires considerably smaller amounts of sample (only few mg) that can be harmlessly obtained by dentists without tooth extraction[67, 68-71].

In this thesis, thermoluminescence (TL) intensity-dose response relation of fluorapatite mineral which is an important apatite mineral in tooth enamel under the different annealing temperatures were investigated.

Firstly, it has been investigated that how the alteration in dose value at different annealing temperature affects the shape of the TL glow curve. As a result of this study, different dose value at different annealing temperature does not affect significantly the shape of glow curve except at 1100°C. The shape of the TL glow curve changes after 616Gy dose value for the sample annealed at 1100 °C. For this dose value and annealing temperature, the wider glow curve becomes narrower glow curve. A distinct peak is located around 180°C. The higher dose value at higher annealing temperature may cause the aggregation of traps. At higher dose values and annealing temperature, there can be a movement of the shallow traps to the near of the active traps.

The second analysis has been done to see the effects of the different dose values at different annealing temperature on the TL peak intensity and area under the glow curves. Dose response is an important experiment in the dosimetric studies for getting knowledge about relationship between TL light output and applied dose. The dose responses of the samples annealed at different annealing temperatures (400°C, 500°C, 600°C, 700°C, 800°C, 900°C, 1000°C and 1100°C ) at fixed annealing time (30min) for different higher doses (154Gy, 308Gy, 616Gy, 1.23kGy and 2.46kGy) have been investigated. A good linearity in dose response is observed in the sample annealed at 400 °C and 700 °C. However, a saturation point is observed at the dose level of 1.23kGy in the graph of sample annealed at 700 °C. The saturation is observed at 616Gy for the samples annealed 800 °C and 900 °C.

The final analysis has been done to see the effects of the different dose values at different annealing temperature on the TL peak temperature. This part of the analysis reveals that the TL peak temperature of the sample annealed at 400 °C and 600 °C shifts to higher temperature region about 20 °C. with increasing dose value. This phenomenon can be explained by the trap conversion. The shallow traps transform to the deeper traps. Therefore, TL peak temperature shifts to the higher temperature region. However, a decreasing in TL peak temperature has been observed with increasing dose value for the samples annealed at 700 °C, 900 °C and 1000 °C (after 616Gy). The TL peak temperature shifts to lower temperature region about 25 °C between 154 Gy and 2.46 kGy. The trap positions close to delocalized bands. In addition, for the samples annealed at 500 °C, 800 °C, 1000 °C (up to 616Gy) and 1100 °C, the TL peak temperature does not affected by the variation of dose value. It means that the trap position or defects position does not change by the variation of dose value. The reason may be that the traps become stable at these annealing temperatures.

In conclusion, the fluorapatite mineral extracted from tooth enamel shows TL properties. Annealing of the sample at different temperatures affects the TL output-dose response relation. A good linearity in dose response is observed in the samples annealed at 400 °C and 700 °C. And also, dose variation differently changes the trap positions at different annealing temperature.

## REFERENCES

- [1] J.L. Bernier, J.G. Muhler, Improving dental practice through preventive measures, The C. V. Mosby Comp., Saint Louis, 1970, pp.139-145.
- [2] J.C. Hess, Endodontie I, II. Librairie Malonine S.A. Paris, 1970.
- [3] H. Sicher, E.L. Dubrul . Oral Anatomy, The C.V. Mosby Company, 1970.
- [4] A.G. Fincham, J. Moradian-Oldak, J.P. Simmer, The structural biology of the developing dental enamel matrix, *J. Struct. Biol.* **126** (1999) 270–299.
- [5] G.A. Macho, Y. Jiang, R. Spears, Enamel microstructure - a truly three-dimensional structure, *J. Human Evol.* **45** (2003) 81–90.
- [6] P. Fourman, P. Royer, J.M. Lewell, B.D. Morgan, Blackwell scientific publication, Oxford, 1968.
- [7] P. Fattibene, F. Callens, EPR dosimetry with tooth enamel: A review, *Applied Radiation and Isotopes* **68** (2010) 2033–2116.
- [8] K. Langeland, T. Tagi, Investigation on the innervation of teeth, *Int. Dent. J.* **22** (1972) 240-269.
- [9] R.Z. LeGeros, Apatites in biological systems, *Prog. Crystal Growth Charact.* **4** (1981) 1–5.
- [10] H. Lanjanian, F. Ziaie, M. Modarresi, M. Nikzad, A. Shahvar, S.A. Durrani, A technique to measure the absorbed dose in human tooth enamel using EPR method, *Radiation Measurements* **43** (2008) 648–650.
- [11] C.E. Secu, M. Cherestes, M. Secu, C. Cherestes, V. Paraschiva, C. Barca, Retrospective dosimetry assessment using the 380°C thermoluminescence peak of tooth enamel, *Radiation Measurements* **46** (2011) 1109-1112.

- [12] G.Y. Lee, A. Srivastava, D.D. D’Lima, P.A. Pulido, C.W. Colwell, J. Arthroplasty, Hydroxyapatite-Coated Femoral Stem Survivorship at 10 Years, **20** (2005) 57–62.
- [13] T. Matsumoto, M. Okazaki, M. Inoue, S. Yamaguchi, T. Kusunose, T. Toyonaga, Y. Hamada, J. Takahashi, Hydroxyapatite particles as a controlled release carrier of protein, *Biomaterials* **25** (2004) 3807–3812.
- [14] D. Ekendahl, L. Judas, L. Sukupova, OSL and TL retrospective dosimetry with a fluorapatite glass-ceramic used for dental restorations, *Radiation Measurements* **58** (2013) 138-144.
- [15] L.C. Oliveira, A.M. Rossi, O. Baffa, A comparative thermoluminescence and electron spin resonance study of synthetic carbonated A-type hydroxyapatite, *Applied Radiation and Isotopes* **70** (2012) 533–537.
- [16] Y. Fukuda, Thermoluminescence in fluorapatite doped with  $\text{Eu}_2\text{O}_3$  and  $\text{PbO}$ , *Radiation Protection Dosimetry* **100** (2002) 321–324.
- [17] A.A. Romanyukha , D.F. Regulla, Aspects of retrospective ESR dosimetry, *Appl. Radiat. Isot.* **47** (1996) 1293-1297.
- [18] Y. Fukuda, T. Tanaka, Thermally Stimulated Exoelectron Emission and Thermoluminescence in  $\text{Ca}_5(\text{PO}_4)_3\text{F}:\text{Eu}$ . In: *Proc.13th Int. Symp. on Exoemission and its Applications*. Jurmala, Latvia, 2000.
- [19] C. Furetta, *Handbook of Thermoluminescence*, World Scientific Publishing, Singapore, 2010.
- [20] J.M. Brady, N.O. Aarestad, H.M. Swarts, In vivo dosimetry by electron spin resonance spectroscopy, *Med. Phys.* **15** (1968) 43–47.
- [21] A. Wieser, H.Y. Göksu, D.F. Regulla, A. Vogenauer, Dose rate assessment in tooth enamel, *Quaternary Science Reviews* **7** (1988) 491-495.
- [22] I. Veronese, N. El-Faramawy, A. Giussani, M.C. Cantone, E.A. Shishkina, H.Y. Göksu, The use of  $\text{Al}_2\text{O}_3:\text{C}$  in Risø OSL single grains attachment system for assessing the spatial dose rate distribution due to incorporation of  $^{90}\text{Sr}$  in human teeth, *Radiat. Prot. Dosim.* **119** (2006) 408–412.

- [23] J. Roman-Lopez , V. Correcher , J. Garcia-Guinea , T. Rivera, I.B. Lozano, Thermal and electron stimulated luminescence of natural bones, commercial hydroxyapatite and collagen, *Spectrochimica Acta Part A: Molecular and Biomolecular Spectroscopy* **120** (2014) 610–615.
- [24] A. Güttler, A. Wieser, EPR-dosimetry with tooth enamel for lowdoses, *Radiation Measurements* **43** (2008) 819–822.
- [25] I. Veronese, P. Fattibene, M.C. Cantone, V. De Coste, A. Giussani, S. Onori, E.A. Shishkina, EPR and TL-based beta dosimetry measurements in various tooth components contaminated by  $^{90}\text{Sr}$ , *Radiation Measurements* **43** (2008) 813–818.
- [26] S. Egersdorfer, A. Wieser, A. Müller, Tooth enamel as a detector material for retrospective EPR dosimetry, *Appl. Radiat. Isot.* **47** (1996) 1299-1303.
- [27] R. Alvarez, T. Rivera, J. Guzman, M.C. Piña-Barba, J. Azorin, Thermoluminescent characteristics of synthetic hydroxyapatite (SHAp), *Applied Radiation and Isotopes* **83** (2014) 192–195.
- [28] Infodentis, <http://www.infodentis.com/tooth-anatomy/tooth-structure.php>
- [29] Skobe Z. (1976). The secretory stage of amelogenesis in rat mandibular incisor teeth observed by scanning electron microscopy. *Calcif. Tissue Res.* **21**, 83–103 [PubMed]
- [30] Robinson C., Brookes S. J., Bonass W. A., Shore R. C., Kirkham J. (1997). Enamel maturation in dental enamel. *Ciba Found. Symp.* **205**, 156–174 [PubMed]
- [31] Smith C. E. (1998). Cellular and chemical events during enamel maturation. *Crit. Rev. Oral Bio. Med.* **9**, 128–161 [PubMed]
- [32] Warshawsky H., Smith C. E. (1974). Morphological classification of rat incisor ameloblasts. *Anat. Rec.* **179**, 423–446 [PubMed]
- [33] Robinson C., Atkinson P. J., Briggs H. D. (1981a). Histology of enamel organ and chemical composition of adjacent enamel in rat incisors. *Calcif. Tissue Int.* **33**, 513–520 [PubMed]

- [34] Rintoul L, Wentrup-Byrne E, Suzuki S, et al. FT-IR spectroscopy of fluoro-substituted hydroxyapatite: strengths and limitations. *J. Mater. Sci. Mater. Med.*, 2007
- [35] Eslami H, Solati-Hashjin M, Tahriri M. The comparison of powder characteristics and physicochemical, mechanical and biological properties between nanostructure ceramics of hydroxyapatite and fluoridated hydroxyapatite. *Mater. Sci. Eng. C*, 2009
- [36] Botter-Jensen L. (1997). Luminescence technique: instrumentation and methods. *Rad. Meas.*, **17**, 749-768.
- [37] Daniels F. and Boyd C. A. (1953). Thermoluminescence as a research tool. *Science*, **117**, 343-349.
- [38] Aitken M. J., Tite M. S. and Reid J. (1964). Thermoluminescent dating of ancient ceramics, *Nature*, **202**, 1032-1033.
- [39] Aitken M. J., Zimmerman D. W. and Fleming S. J. (1964). Thermoluminescent dating of ancient pottery, *Nature*, **219**, 442-444.
- [40] Mejdahl V. (1969). Thermoluminescence dating of ancient Danish ceramics. *Archaeometry*, **11**, 99-104.
- [41] Wintle A. G. and Huntley D. J. (1980). Thermoluminescent dating of ocean sediments. *Canadian journal of earth sciences*, **17**, 348-360.
- [42] Wintle A. G. (1985). Anomalous fading of thermoluminescence in mineral samples, *Nature*, **245**, 143-144.
- [43] Wintle A. G. (1985). Thermal quenching of thermoluminescence in quartz, *Geophys. J. R. Ast. Soc.*, **41**, 107-113.
- [44] Hasan, F., Kitis, G. and Charalambous, S., *Nucl. Instrum. Methods* **B9**, 218 (1985)
- [45] Pradhan, A.S., *Radiat. Prot. Dosim.* **47**, 151 (1993)
- [46] Drisoll, C.M.H., Fisher, E.S., Furetta, C., Padovani, R., Richards, D.J. and Wall, B.F., *Radiat. Prot. Dosim.* **6**, 305 (1984)

- [47] Schulman, J.H., Kirk, R.D. and West, E.J., In: Proc. Int. Conf. on Luminescence Dosimetry, Stanford. CONF 650637, p. **113** (1967).
- [48] Prokic, M.S., Health Phys. **42**, 849 (1982).
- [49] Wilson, C.R. and Cameron, J.R., In Proc. 5<sup>th</sup> Int. Conf. on Luminescence Dosimetry, Sao Paulo, p. **161** (1971).
- [50] Takenaga, M., Yamamoto, O. and Yamashita, T., Health Phys. **44**, 387 (1983)
- [51] Portal, G., In: Applied Thermoluminescence Dosimetry, eds M. Oberhofer and A. Scharmann (Adam Hilger, Bristol) p.**97** (1981)
- [52] Pradhan, A.S., Bhatt, R.C. and Vohra, K.G., Bull. Radiat. Prot. **5**, 13 (1982)
- [53] Bahbout, S. and Furetta, C., Radiat. Prot. Dosim. **4**, 43 (1983)
- [54] Oduko, J.M., Harris, S.J. and Stewart, J.C., Radiat. Prot. Dosim. **8**, 257 (1984)
- [55] Szabo, P.P., Pradhan, A.S. and Chandra, B., Int. J. Appl. Radiat. Isot. **35**, 415 (1984)
- [56] Jones, A.R., Radiat. Prot. Dosim. **6**, 71 (1984)
- [57] Ogunleye, O.T., Richmond, R.G. and Cash, L.B., Health Phys. **49**, 527 (1985)
- [58] Richmond, O.T., Ogunleye, O.T., Cash, B.L. and Jones, K.L., Appl. Radiat. Isot. **38**, 313 (1987)
- [59] Prokic, M., Radiat. Prot. Dosim. **17**, 393 (1986)
- [60] Driscoll C.M.H., National Radiological Protection Board, *Tech. Mem.* **5**, 82.
- [61] Busuoli G. 1981. In Applied Thermoluminescence Dosimetry. Bristol: Adam Hilger publisher
- [62] Driscoll C.M.H., Barthe J.R., Oberhofer M., Busuoli G. and Hickman C. (1986). Annealing procedures for commonly used radiothermoluminescent materials. *Rad. Prot. Dos.* **14** (1), 17-32.
- [63] EsenGün (2006). Investigation of Thermoluminescence Properties of Calcite



(CaCO<sub>3</sub>). Engineering Physics University of Gaziantep

- [64] Harshaw TLD<sup>TM</sup> Model 3500. (2014). <http://www.thermoscientific.com/>
- [65] 9010 Optical Dating System User Manual, Dec. 1993.
- [66] Model 3500 Manual TLD Reader User's Manual, July 30 1994
- [67] Brady, J.M., Aarestad, N.O., Schwartz, H.M., 1968. in vivo dosimetry by electron spin resonance spectroscopy. *Health Phys.* **15**, 43-47
- [68] Driessens, F.C.M., 1980. The mineral in bone, dentine and tooth enamel. *Bull. Soc. Chim. Belg.* **89**, 663e689.
- [69] Moens, P., De Volder, P., Hoogewijs, R., Callens, F., Verbeeck, R., 1993. Maximum-likelihood common-factor analysis as a powerful tool in decomposing multi-component EPR powder spectra. *J. Magn. Reson.* **101**, 1-15.
- [70] Callens, F., Vanhalewyn, G., Matthys, P., Boesman, E., 1998. EPR of carbonate derived radicals: applications in dosimetry, dating and detection of irradiated food. *Appl. Magn. Reson.* **14**, 235-254
- [71] International Atomic Energy Agency, 2002. Use of Electron Paramagnetic Resonance Dosimetry with Tooth Enamel for Retrospective Dose Assessment. IAEA, IAEA-TECDOC-1331, Vienna, ISBN 92-0-119402-1